SI Results

A 7-weeks rapamycin treatment regimen did not modify altered DNA methylation in sperm of aged mice. To begin to address whether rapamycin treatment of old fathers has an effect on DNA methylation changes in their sperm, we subjected young (3 months old) and old (22 months old) mice to a 7-weeks treatment with either rapamycin or vehicle control prior to sperm collection (**Fig. S8A**). Notably and consistent with earlier observations (1), rapamycin had a strong suppressive effect on spermatogenesis, resulting in lower sperm counts in treated mice compared to vehicle controls (**Fig. S8B**). We focused our analysis of age-related DNA methylation changes on a ~2kb genomic region upstream of and overlapping with *Gm7120* which was among the top hypermethylated regions in old father sperm as well as old father offspring tissue (**Tables S1** and **S7**). Targeted bisulfite sequencing of this area confirmed CpG hypermethylation in old father sperm (**Fig. S8C,D**). Our data indicate that a 7-weeks rapamycin treatment regimen was insufficient to modify age-related hypermethylation of this genomic region (**Fig. S8C,D**). It remains to be determined if a longer-term rapamycin treatment during the course of natural aging prevents age-related differential methylation at this locus. Additionally, further studies are required to address whether rapamycin treatment, either short-term or more chronic in nature, can influence age-related epigenetic changes at other genomic positions.

Immune system changes in old father offspring mice. The epigenetic and transcriptional analyses outlined above also highlight alterations in immune regulators (including mTOR-related cell signaling) in aged fathers and their offspring. To address whether these were associated with changes in the composition of immune cell populations in old father offspring mice, we quantified leukocyte populations in the peripheral blood of OFO and YFO mice. We noted an increased abundance of several T cell subpopulations in OFO mice, including $CD44^{high}$-expressing $CD4^{+}$ T cells and $CD44^{high}$-expressing $CD8^{+}$ T cells, indicating an increase in the proportion of activated/memory T cells in these animals (**Fig. S9**). The cellular

changes are in line with observations in mice with altered mTOR signaling (1, 2). Together, these data are consistent with the pro-inflammatory transcriptional changes in OFO mice and suggest an altered immunological state in these animals.

Metabolic alterations in old father offspring mice. We also determined plasma glucose and lipid concentrations in young and old father offspring mice. These analyses showed changes in the temporal plasma glucose profile following bolus glucose injection in OFO mice (**Fig. S10A**), as well as elevated plasma cholesterol concentrations (**Fig. S10B**) in OFO mice compared to YFO animals. These findings indicate that metabolic alterations could contribute to aging trajectories in OFO mice.

Altered learning and memory in old father offspring mice. Because our data revealed epigenetic, gene expression and biochemical changes in hippocampal tissue of old father offspring mice, we included in our analyses an assessment of learning and memory as a function of paternal age. First, we performed a meta-analysis of a large fear conditioning dataset that involved mice with a range of different parental ages (for details, see **SI Methods**). Stratification of the dataset by paternal age revealed an inverted U-shaped relationship of paternal age and freezing behavior in offspring mice (**Fig. S11A**) which is akin to previously reported paternal age effects on measures of cognitive function in humans (3-5). In contrast, we did not note any obvious maternal age effect on freezing behavior in offspring when we stratified the dataset by maternal age (with the range of maternal ages being limited due to age-related infertility in females) (**Fig. S11B**). We also analyzed spatial learning in the Morris water maze and in an object-place-recognition learning task in offspring derived from either young or old fathers (for details, see **SI Methods**). Our analyses showed decreased probe trial-associated target quadrant occupancy in the Morris water maze in OFO mice (for details, see **SI Methods** and **Fig. S11C**-**E**). OFO mice also showed similar exploration times of an object relocated to a novel position and an object in a familiar location during a probe trial in an object-place-recognition learning task (for details, see **SI Methods**

and **Fig. S11F**). Together, these data add to growing evidence indicating paternal age effects on behavior and cognitive functions in animal models, as well as in humans (3-9).

SI Discussion

We found a subset of traits to differ between the young adult YFO and OFO group (e.g. plasma cholesterol, learning and memory), while other differences emerged during the course of natural aging in YFO and OFO mice (many histopathological measures), suggesting that these differences reflect an altered aging rate in OFO mice (i.e., an altered trajectory of the age-dependent change in the corresponding parameters). Together with our epigenetic findings this observation raises the possibility that inherited aging-associated epigenetic changes in the male germline influence the trajectory of age-dependent tissue changes in the next generation.

Stratification of a large fear conditioning dataset by paternal age suggested that freezing behavior in offspring is highest in offspring of fathers of an intermediate age range (3-12 months) and is reduced in offspring of older fathers (>12 months), as well as in offspring of very young fathers (<3 months) (**Fig. S11A**). Interestingly, such an inverted U-shaped relationship of paternal age and offspring traits has also been observed with regards to cognitive outcome measures in human populations (3-5). These findings indicate that very young paternal ages may also be associated with phenotypic consequences in the next generation. Future studies should examine the scope of these effects and assess sperm epigenetic profiles during sexual maturation (i.e., comparing adolescent and adult mice).

Our study identified epigenetic and phenotypic changes in the F1 offspring of old fathers. It remains to be determined if the F2 offspring of old fathers feature epigenetic and/or phenotypic alterations similar to the ones described here for F1 progeny. The observation

that *Gm7120*-associated sequences overlapping with the ones that we found to be hypermethylated in old father sperm and in old father offspring tissue are resistant to demethylation in primordial germ cells (10, 11) suggests that at least some of the age-related epigenetic changes might be passed on to second generation offspring.

SI Methods

FACS-based analysis of peripheral blood leukocytes. FACS-based analyses of leukocyte populations in the peripheral blood were performed as previously described (1). The cell pellet isolated from whole blood was dissolved in NH4Cl-based, Tris-buffered erythrocyte lysis solution. After washing and blocking steps, cells were stained with fluorescence-conjugated monoclonal antibodies (Pharmingen) and propidium iodide was added for the identification of dying/dead cells. Cells were sorted using a three-laser 10-color flow cytometer (LSRII, Becton Dickinson; Gallios, Beckman Coulter). Living cells were gated using their SSC/CD45 signal to isolate leukocyte populations. A total number of 10,000-30,000 living CD45+ cells per sample were analyzed. We analyzed the abundance of T cells ($CD3^+$), $CD4^+$ T cells, $CD8^+$ T cells, $CD25^+$ $CD4^+$ T cells, γδ T cells, $CD44^{high}$-expressing $CD4^+$ T cells, $CD44^{high}$-expressing $CD8^+$ T cells, CD62L-expressing $CD4^+$ T cells, as well as CD62L-expressing $CD8^+$ T cells in young father offspring mice and old father offspring animals (YFO, n = 27 mice from 11 litters; OFO, n = 29 mice from 10 litters). Statistical analyses were performed using unpaired, two-tailed t-tests.

Intraperitoneal glucose tolerance test and plasma cholesterol concentration measurements. For the intraperitoneal glucose tolerance test (YFO, n = 27 mice from 11 litters; OFO, n = 29 mice from 10 litters), food was withdrawn overnight. Mice were injected intraperitoneally with 2 g glucose/kg body mass and blood samples were collected from the tail tip at 15, 30, 60 and 120 min after glucose injection. Data were analyzed by two-way ANOVA with the

between-subjects factor paternal age and the within-subjects factor time point. Plasma cholesterol concentrations were measured using a Beckman-Coulter AU 480 autoanalyzer (YFO, *n* = 27 mice from 11 litters; OFO, *n* = 29 mice from 10 litters). Statistical analysis was performed using an unpaired, two-tailed t-test.

Behavior. To begin to test for possible paternal age effects on learning and memory, we performed a meta-analysis of a large fear conditioning dataset in WT mice (mixed BL/6-129 genetic background), which we stratified by paternal age (in 3 months age bins; for numbers of animals, see **Fig. S11A**). After a two-minute baseline, mice were subjected to tone-signaled conditioning (30s tone co-terminating with a 2s, 0.75 mA shock) (12). Freezing levels assessed during the last two minutes of the fear conditioning session were compared across paternal age groups via one-way ANOVA. The hidden version of the Morris water maze was performed as previously described (13) with the following modifications: After handling, F1 offspring of old and young fathers (YFO, *n* = 25 mice from 10 litters; OFO, *n* = 17 mice from 7 litters) received 2 daily training trials for 7 consecutive days. Escape latencies were analyzed by two-way ANOVA with the between-subjects factor paternal age and the within-subjects factor training day. To evaluate the accuracy with which the animals had learned the position of the escape platform, we performed probe trial analyses comparing the time that mice spent searching in the target quadrant (which previously contained the escape platform) vs. the other quadrants. An overall analysis of quadrant occupancies was carried out by two-way ANOVA with the between-subjects factor paternal age and the within-subjects factor quadrant. Additionally, swim speed and target quadrant occupancy were analyzed by unpaired t-test (OFO vs. YFO). The object-place-recognition learning task was conducted as previously described (1). In brief, after handling and habituation to the test arena, animals (YFO, *n* = 16 mice from 6 litters; OFO, *n* = 14 mice from 6 litters) received a single 16-min training session during which two identical objects (small glass bottles) were placed in defined locations of the test arena. On the next day, we performed a single test session, in the context of which one of the objects was moved to a new location, while the position of the

other object remained unaltered. The time the animals spent exploring the object in the novel location and the known location during the test was hand-scored by an experienced observer from the videotape. Exploration times were analyzed by two-way ANOVA with the between-subjects factor paternal age (OFO/YFO) and the within-subjects factor object location (novel/familiar). Additionally, exploration times of the object in the novel vs. familiar location were compared by unpaired t-tests within groups (OFO, YFO).

Histology-based fluorescence intensity analyses. Histology-based fluorescence intensity analyses were carried out to assess the phosphorylation of ribosomal protein S6 at Ser240/244 within spermatogenic cell lineages in testis derived from young (3 months old) and old (20 months old) C57BL/6J Rj mice. Tile scan Z stack maximum intensity projections were collected from immunolabeled testis sections (12 µm thick) by collecting a 6 x 6 array of 1024 x 1024 resolution confocal images (Zeiss LSM 700). ROIs of the seminiferous tubules were made by a researcher blind to experimental condition in stitched mosaic images leaving the basal spermatogonia layer excluded from the ROI. Then total corrected fluorescence intensity was measured from all ROIs in the p-S6 channel (488 wavelength) using the CTCF method (14), taking into account background fluorescence. Because the number of cells contained in the seminiferous tubules could bias the average intensity results, we calculated the average cell number per tubule by using the auto threshold in FIJI (ImageJ, NIH) and then applying the waterfall binary correction to differentiate profiles that contact each other, and then obtaining a DAPI profile count only inside of the previously generated ROIs. The background corrected fluorescence was then normalized to the average cell number per tubule for that image. Data from young and old animals were analyzed by unpaired t-test.

Rapamycin effects on aged sperm. To examine the effects of rapamycin on DNA methylation changes in aged sperm, we treated young (3 months old; n = 9 mice per group) and old male C57BL/6J Rj mice (22 months old; n = 9 mice for the rapamycin-treated group and n = 5 mice for the vehicle-treated group) with either oral rapamycin or vehicle control for a period of 7

weeks prior to sperm collection. Statistical analyses of sperm counts were performed by two-way ANOVA with the between-subjects factors age (young/old), as well as treatment (rapamycin/vehicle).

Primary antibodies used for Western blots. The following primary-antibodies were used for immunoblotting: rabbit monoclonal anti-mTOR (clone 7C10, 1:2000, Cell Signaling Technology, catalog no. 2983), rabbit monoclonal anti-Raptor (clone 24C12, 1:1000, Cell Signaling Technology, catalog no. 2280), rabbit monoclonal anti-Rictor (clone 53A2, 1:1000, Cell Signaling Technology, catalog no. 2114), rabbit monoclonal anti-phospho-4E-BP1 (Thr37/46) (clone 236B4, 1:2000, Cell Signaling Technology, catalog no. 2855), rabbit monoclonal anti-4E-BP1 (clone53H11, 1:2000, Cell Signaling Technology, catalog no. 9644), rabbit monoclonal anti-phospho-p70S6 Kinase (Thr389) (clone 108D2, 1:2000, Cell Signaling Technology, catalog no. 9234), rabbit monoclonal anti-p70S6 Kinase (clone 49D7, 1:4000, Cell Signaling Technology, catalog no. 2708), rabbit polyclonal anti-phospho-S6 ribosomal protein (Ser240/244) (1:2000, Cell Signaling Technology, catalog no. 2215), mouse monoclonal anti-S6 ribosomal protein (clone 54D2, 1:1000, Cell Signaling Technology, catalog no. 2317), mouse monoclonal anti-nitrotyrosine (clone 1A6, 1:10000, Merck Millipore, catalog no. 05-233), mouse monoclonal anti-actin (clone C4, 1:20000, MP Biomedicals, catalog no. 0869100).

Mice for Ribotag experiments. *Tsc2*$^{+/-}$ mice were generated as previously described (15) and were kept on a C57BL/6NCrl genetic background. The generation of Ribotag mice (16) and αCaMKII-Cre mice (17) (both lines were on a C57BL/6J genetic background) was also previously described. We crossed the αCaMKII-Cre and Ribotag lines and selected female offspring positive for both transgenes for an additional cross with male *Tsc2*$^{+/-}$ mice. Experimental animals, used for gene expression analyses, were *Tsc2*$^{+/-}$ mutants and the corresponding wildtype littermate controls on the αCaMKII-Cre/Ribotag background.

To assess the effects of rapamycin on hippocampal neuronal gene expression, we subjected

198 *Tsc2*$^{+/-}$/αCaMKII-Cre/Ribotag mice and WT/αCaMKII-Cre/Ribotag mice to rapamycin or
199 vehicle control treatment for a period of 6 weeks prior to sacrifice (rapamyin-treated *Tsc2*$^{+/-}$
200 /αCaMKII-Cre/Ribotag, *n* = 4 mice; vehicle-treated *Tsc2*$^{+/-}$/αCaMKII-Cre/Ribotag, *n* = 3 mice;
201 rapamycin-treated WT/αCaMKII-Cre/Ribotag, *n* = 5 mice; vehicle-treated WT/αCaMKII-
202 Cre/Ribotag, *n* = 5 mice).
203
204 *Ribotag immunohistochemistry*. Mouse brain halves were immersion fixed in formalin and
205 embedded in paraffin. Four µm thick sections were deparaffinized through a series of
206 xylenes and decreasing concentrations of ethanol. Epitope retrieval was performed using a
207 vegetable steamer with slides in 10 mM citrate buffer, pH 8.0, for 30 minutes, then allowed to
208 cool to room temperature. Endogenous peroxidase activity was quenched with 0.3% H_2O_2 for
209 30 minutes. Endogenous immunoglobulins were masked using a Mouse-on-Mouse
210 horseradish peroxidase kit from Vector Labs (PK-2200) following the manufacturer's
211 protocol. HA-7 antibody targeting the HA epitope of the RiboTag protein was purchased from
212 Sigma (catalog no. H9659) and used at a 1:2000 dilution. Enzymatic substrate NovaRed
213 from Vector Labs (SK-4800) was reacted for ~2 minutes, and sections were subsequently
214 counterstained with hematoxylin, dehydrated, and cover slips were mounted with depex.
215 Images were collected with Zen light software and a Zeiss AxioCam MRc camera mounted
216 on a Zeiss Axio inverted microscope.
217
218 *Ribotag immunoprecipitation*. Cell-type-specific isolation of ribosome-associated mRNA from
219 hippocampi of αCaMKII-Cre/Ribotag mice was performed essentially as described before
220 (16) but with a few modifications. In contrast to the original protocol, heparin was excluded
221 from the polysome buffer, and supernatant was pre-cleared with magnetic beads, then
222 incubated with anti-HA antibody 12CA5 (Roche Life Science), followed by incubation
223 with fresh magnetic beads. Quality and quantity of immunoprecipitated mRNA and total RNA
224 isolated from the input supernatant were verified by Qubit (Qubit RNA HS Assay Kit, Thermo
225 Fisher Scientific) and Agilent 2100 Bioanalyzer (Agilent RNA 6000 Pico Kit, Agilent

Technologies). The following number of samples was processed and subjected to RNA-seq: rapamycin-treated *Tsc2*$^{+/-}$/αCaMKII-Cre/Ribotag, *n* = 4 mice; vehicle-treated *Tsc2*$^{+/-}$/αCaMKII-Cre/Ribotag, *n* = 3 mice; rapamycin-treated WT/αCaMKII-Cre/Ribotag, *n* = 5 mice; vehicle-treated WT/αCaMKII-Cre/Ribotag, *n* = 5 mice.

Analysis of mutation rates. Mutation rates were estimated by calling private variants using GATK (18) in RNA-seq data obtained from young and old father offspring animals (at 4 weeks of age; hippocampus as starting material; YFO, *n* = 6 mice from 6 litters; OFO, *n* = 6 mice from 6 litters). A base was declared as sufficiently covered in a sample if it had a depth of at least 20x. A mutation was included if (i) it had at least 20x coverage in a given sample, (ii) the genotype only existed in one sample, (iii) all of the other samples had coverage at that base and (iv) the genotype quality was 99 or greater. We compared estimated mutation rates across groups by unpaired, two-tailed t-test.

Analysis of F1 hippocampus telomere length. qRT-PCR was used to compare the values of relative telomere length of mouse hippocampal DNA between offsprings of young and old fathers according to the protocol of (19, 20). Relative telomere length (T/S) was expressed as a ratio of telomere repeat copy number (T) to a control single copy number gene (36B4) (S). qRT-PCR, was performed for both telomeres and 36B4 using 20 ng DNA samples in the same 96-well plate. Each reaction of the assay was of 25 µl total volume and included 12.5 µl Sybr Green PCR Master Mix (Applied Biosystems). For telomere, 300 nM of each of the forward and reverse primers (Sigma, UK) were employed. Forward and reverse telomeric primers were 5′ CGG TTT GTT TGG GTT TGG GTT TGG GTT TGG GTT TGG GTT 3′ and 5′ GGC TTG CCT TAC CCT TAC CCT TAC CCT TAC CCT TAC CCT 3′ respectively. For 36B4 gene, 300 nM forward primer, 500 nM reverse primer were utilized. Forward and reverse primers for the 36B4 portion of the assay were 5′ ACT GGT CTA GGA CCC GAG AAG 3′ and 5′ TCA ATG GTG CCT CTG GAG ATT 3′, respectively. The reaction was performed on a lightcycler-480 (Roche) with the following conditions: 95°C for 10 minutes, followed by 40

repeats of 95°C for 15 seconds and 56°C for 1 minute, followed by a dissociation stage to monitor amplification specificity. qRT-PCR results were exported to Excel (Microsoft, Redmond, WA) and analyzed. The relative telomere length (T/S) was calculated as previously described in (19, 20). An unpaired, two-tailed t-test was then conducted to compare relative telomere length between offspring of young and old fathers.

RNA sequencing. RNA was extracted from individual mouse hippocampi or testes with an RNeasy kit (Qiagen) following the manufacturer's instructions. RNA from hippocampi were quality controlled by using qPCR to ensure that samples were not contaminated by tissue from the choroid plexus. Towards this end, RNA was reverse transcribed into cDNA and the levels of a number of choroid plexus marker genes were assessed using specific TaqMan probes. The delta delta Ct method with Actb was used to assess relative expression. Next, we determined quality and quantity of input RNA with a 2100 Bioanalyzer (Agilent Technologies) using the RNA 6000 Nano or Pico Kit, respectively. Input RNA was then used to create a next generation sequencing library (Illumina). All libraries were run on an Illumina HiSeq2000TM (50 bp single end sequencing). After sequencing, adapters were trimmed and low quality (Phred < 5) bases removed and the results aligned with STAR (21). Per-gene counts were then generated with featureCounts (22) and statistics computed with DESeq2 (23). All p-values were adjusted for multiple comparisons using the Benjamini and Hochberg method. We used Ingenuity Pathway Analyses (Qiagen) to identify pathways with significant enrichment among sets of differentially expressed genes.

Small RNA sequencing. Total RNA from sperm was isolated using TRIzol reagent in conjunction with the PureLink RNA Mini Kit (Ambion) according to the manufacturer's instructions. RNA was used to create a next generation sequencing library (TruSeq Stranded Total RNA with Ribo-Zero Human/Mouse/Rat Library Prep Kit, Illumina). Libraries were then run on an Illumina HiSeq2000TM. The small RNA-seq data was analyzed using Oasis 2 (24) (Rahman *et al.*, Bioinformatics, *in revision*). For differential expression we used the 'DE

282 analysis' module of Oasis, considering small RNAs significantly differentially expressed when
283 their adjusted p-value was smaller than 0.05. Potential targets of differentially expressed
284 miRNAs were annotated using the experimentally validated microRNA-target interaction
285 database – miRTarBase (25).
286
287 *Functional analysis of miRNA targets*. We performed enrichment analysis of pathway-based
288 sets of proteins considering all the validated targets from up- and down-regulated miRNAs.
289 Enrichment analysis was done employing ConsensusPathDB (26) by using the
290 'overrepresentation analysis' online tool. As input, we uploaded the 'Gene Symbol' protein
291 identifiers of each target set. We searched against pathways as defined by KEGG (27), with
292 a minimal overlap with the input list of 2 and a p-value cutoff of 0.01. Also, employing the
293 same website and the same analysis tool, we performed an enrichment analysis based on
294 Gene Ontology (28) level 4 category of biological processes, molecular function and cellular
295 component. For this analysis, we considered only the identified core proteins and set the p-
296 value cutoff at 0.01.
297
298 *Repeat element expression analysis*. Samples were adapter and quality trimmed and then
299 aligned with STAR (21), allowing up to 1000 alignments per read. These alignments were
300 grouped by read name, allowing them to be processed as a group and subset such that only
301 alignments with the highest alignment scores in a group were further considered. If any
302 alignment in the group overlapped with a known exon (Ensembl, release 79) then the entire
303 group was presumed to have originated from that gene and excluded from further analysis.
304 For each remaining group, the alignments were tested for overlaps with the UCSC
305 repeatmasker track for mm10, after chromosome name conversion. If no alignments in a
306 group overlapped with an annotated repeat then the group was excluded from further
307 analysis. If all the alignments that overlapped a repeatmasker entry shared the same
308 repName/repClass/repFamily ID, then the counter for that repName/repClass/repFamily was
309 incremented. The source code for this procedure is freely available online

(https://github.com/dpryan79/countRepeats). For repClass and repFamily, approximately 5% of read groups overlapped more than one ID. For repName, this figure was approximately 20%. Output unique counts were then entered into DESeq2 (23) for further analysis.

Reduced representation bisulfite sequencing. Frozen sperm and hippocampi were briefly ground in lysis buffer and then DNA extracted with TRIzol (Life Technologies) in phase lock gel tubes (5 Prime) following the manufacturer's recommendation. After extraction, samples were run on an agarose gel to ensure sample integrity. Library preparation and sequencing was performed in collaboration with a specialized service company (Zymo Research). EpiQuest libraries were prepared from 200-500 ng genomic DNA digested with 60 units of TaqI and 30 units of MspI (NEB) sequentially. Size-selected TaqI-MspI fragments (40–120 bp and 120–350 bp) were filled in and 3'-terminal-A extended, extracted with Zymo Research DNA Clean & Concentrator kit. Ligation to pre-annealed adapters containing 5'-methyl-cytosine instead of cytosine (Illumina) was performed using the Illumina DNA preparation kit and protocol. Purified, adaptor ligated fragments were bisulphite-treated using the EZ DNA Methylation-Direct Kit (Zymo Research). Preparative-scale PCR was performed and DNA Clean & Concentrator-purified PCR products were subjected to a final size selection on a 4% NuSieve 3:1 agarose gel. SYBR-green-stained gel slices containing adaptor-ligated fragments of 130-210 bp or 210-460 bp in size were excised. Library material was recovered from the gel (Zymoclean Gel DNA Recovery Kit, Zymo Research) and sequenced on an Illumina HiSeq 2000. After sequencing, adapters and low quality bases were trimmed from reads before mapping against the mouse genome with Bison (29). Before extraction of per-C methylation metrics, methylation bias plots were constructed and regions showing biased methylation conversion from both ends of each read were excluded from further use. Methylation counts were then loaded into R and a paired-weighted T-test, where weights were the minimum of the coverage of the groups, used to calculate the statistics of each region of interest. All p-values were adjusted for multiple comparisons using the Benjamini and Hochberg method. Differentially methylated promoters were defined as promoters

(distance to TSS between -5 kb and +1 kb) overlapping with a 2-kb differentially methylated region. Assessment of the significance of dataset overlap between F0 and F1 differentially methylated regions was performed based on exact hypergeometric probability. We used Ingenuity Pathway Analyses (Qiagen) to identify pathways with significant enrichment among sets of genes with differentially methylated promoters.

Targeted bisulfite sequencing. Sperm DNA was extracted using the Quick-DNA Microprep Plus Kit (Zymo Research) according to the manufacturer's instructions with the following modifications. In brief, sperm pellets were resuspended in up to 50 µl PBS and homogenized in the presence of 50 µl BioFluid & Cell Buffer (Red). Samples were incubated for 1 h at 55°C and 450 rpm with 5 µl Proteinase K, followed by a second incubation step (1 h, 55°C, 450 rpm) after the addition of 10 µl 0.5 M Bond-Breaker TCEP Solution (Thermo Fisher Scientific). Digested samples were mixed with 115 µl Genomic Binding Buffer and transferred to a Zymo-Spin IC-XM Column. Washing was performed according to the protocol (Zymo Research) and pure DNA was eluted in DNase-free water. Targeted DNA methylation analyses were then carried out in collaboration with a specialized service company (Zymo Research). Assays were designed targeting CpG sites within the specified regions of interest upstream of and overlapping with *Gm7120* (chr13: 120276057-120277892; mm9 coordinates) using primers generated with Rosefinch, Zymo Research's proprietary sodium bisulfite converted DNA-specific primer design tool. Information on primers used is provided in a separate document (Supplementary_Material_Targeted_BS-Seq_Primers.xlsx). All primers were resuspended or ordered in TE solution at 100 µM. Primers were then mixed (if necessary) and diluted to 2 µM each. All primers were tested using Real-Time PCR with 1 ng of bisulfite-converted control DNA, in duplicate individual reactions. Following primer validation, samples were bisulfite converted using the EZ DNA Methylation-Lightning Kit (Zymo Research, catalog no. D5030) according to the manufacturer's instructions. Multiplex amplification of all samples using region of interest-specific primer pairs and the Fluidigm Access Array System was performed following the manufacturer's instructions. The resulting

amplicons were pooled for harvesting and subsequent barcoding according to the Fluidigm instrument's guidelines. After barcoding, samples were purified (ZR-96 DNA Clean & Concentrator, Zymo Research, catalog no. D4023) and then prepared for massively parallel sequencing using a MiSeq V2 300bp Reagent Kit and paired-end sequencing protocol according to the manufacturer's instructions.

After sequencing, sequence reads were identified using standard Illumina base-calling software, followed by analysis with a Zymo Research proprietary analysis pipeline. Low quality nucleotides and adapter sequences were trimmed off during analysis QC. Sequence reads were aligned to the reference genome using Bismark (30). The methylation level of each sampled cytosine was estimated as the number of reads reporting a C, divided by the total number of reads reporting a C or T. We used two-way ANOVA with the between-subjects factors age and treatment to compare average methylation ratios in the region of interest across groups.

ChIP sequencing. Frozen sperm pellets were resuspended in 500 µL of somatic cell lysis buffer (SCLB: 0.1 % SDS, 0.5 % Triton X-100, 50 mM DTT in 10 mM Tris pH 7.5) and incubated on ice for 20 min. The sperm was pelleted by 3 min of centrifugation at 2,000 g and quickly washed once in 500 µL of Nelson buffer (150 mM NaCl, 20 mM EDTA (pH 8), 50 mM Tris (pH 7.5), 0.5% NP-40, 1% Triton-X-100 and Roche Complete protease inhibitors). The pellet was then resuspended in 100 µL Complete Lysis Buffer (CLB: 15 mM Tris-HCl (pH 7.5), 60 mM KCl, 5 mM MgCl2, 0.1 mM EGTA, 0.3 M sucrose and 0.5 mM DTT). The same volume of Lysis Buffer plus Detergent (CLB with 0.5 % NP40 and 1% sodium deoxycholate) was added and the mix was incubated on ice for 10 min. One volume of MNase buffer (85 mM Tris (pH 7.5), 3 mM MgCl2, 2 mM CaCl2, 0.3 M sucrose) with MNase (NEB M0247S, final 1/2000) was added and the mix was incubated for 15 min at 37°C with 800 rpm shaking. The reaction was stopped on ice by adding EDTA to 5 mM. Protease inhibitors (Roche) were added as well as 120 mM NaCl, 1% NP-40 and 0.1% SDS. The chromatin was pre-cleared

with 20 µL of BSA-blocked Protein A Dynabeads (Life Technologies) for 1 h at 4°C. The rest of the ChIP protocol was previously published (31). We used 0.5 µg H3K4me3 antibody (Abcam ab8580, lot number GR126420-2) and 0.5 µg H3K27me3 (Abcam ab6002).

In order to determine the best ChIP conditions for sperm, modifications of this protocol were tested: The frozen sperm pellets were resuspended in PBS and fixed by 1% formaldehyde (Sigma) for 5 min. The reaction was quenched by adding glycine to 125 mM. The pellets were washed in 500 µL of Nelson buffer and sheared either by sonication or by MNase digestion (as above). For the sonication, the pellets were resuspended in 100 µL of RIPA (140 mM NaCl, 1 mM EDTA, 1% TritonX-100, 0.1% sodium deoxycholate, 10 mM Tris-Cl (pH 8.0), 1% SDS and protease inhibitors), incubated for 10 min at 4°C and sheared in a Bioruptor Plus (Diagenode) for 20 cycles, 30 s ON/OFF. The chromatin was cleared by centrifugation at 16,000 g for 5 min at 4°C and diluted in IP buffer (31). The comparison of the different sperm ChIP protocols showed that the native ChIP protocol using MNase digestion on unfixed chromatin yielded the best results (**Fig. S2**). The ChIP-seq libraries were prepared using Digenode Microplex kit as previously described (31).

ChIP-seq data was first subjected to quality control as described previously obtaining high-quality uniquely and multi-mapped reads (31). Peaks and differentially occupied regions were detected as previously described (31). In brief, MACSv2.0.10 (32) was used to compare ChIP-seq signal to a corresponding whole-cell extract sequenced control (input) to identify narrow regions of enrichment (peaks) that pass a Poisson adjusted p-value threshold of 0.05. Fragment lengths for each data set were pre-estimated using the in-house R package ‘chequeR’ and these fragment length estimates were explicitly used as parameters in the MACS2 program (–shift-size = fragment_length/2).

To have a common set of peaks for each histone modification, all the replicates were concatenated and merged using bedtools mergeBed (33). Significant changes between

peaks in old and young father sperm histone modifications were assessed with DESeq2 (23). For differential histone post-translational modifications, only peak regions with an adjusted p-value < 0.05 were annotated and considered for further analysis.

Data deposition. Next-generation sequencing datasets have been deposited to ENA under the study accession number PRJEB23859.

References

1. Neff F, *et al.* (2013) Rapamycin extends murine lifespan but has limited effects on aging. *J Clin Invest* 123(8):3272-3291.
2. Zhang S, *et al.* (2011) Constitutive reductions in mTOR alter cell size, immune cell development, and antibody production. *Blood* 117(4):1228-1238.
3. Auroux MR, *et al.* (1989) Paternal age and mental functions of progeny in man. *Hum Reprod* 4(7):794-797.
4. Malaspina D, *et al.* (2005) Paternal age and intelligence: implications for age-related genomic changes in male germ cells. *Psychiatr Genet* 15(2):117-125.
5. Saha S, *et al.* (2009) Advanced paternal age is associated with impaired neurocognitive outcomes during infancy and childhood. *PLoS Med* 6(3):e40.
6. Auroux M (1983) Decrease of learning capacity in offspring with increasing paternal age in the rat. *Teratology* 27(2):141-148.
7. Garcia-Palomares S, *et al.* (2009) Long-term effects of delayed fatherhood in mice on postnatal development and behavioral traits of offspring. *Biol Reprod* 80(2):337-342.
8. Malaspina D, Gilman C, & Kranz TM (2015) Paternal age and mental health of offspring. *Fertil Steril* 103(6):1392-1396.
9. Smith RG, *et al.* (2009) Advancing paternal age is associated with deficits in social and exploratory behaviors in the offspring: a mouse model. *PLoS One* 4(12):e8456.
10. Guibert S, Forne T, & Weber M (2012) Global profiling of DNA methylation erasure in mouse primordial germ cells. *Genome Res* 22(4):633-641.
11. Kobayashi H, *et al.* (2013) High-resolution DNA methylome analysis of primordial germ cells identifies gender-specific reprogramming in mice. *Genome Res* 23(4):616-627.
12. Matynia A, *et al.* (2008) A high through-put reverse genetic screen identifies two genes involved in remote memory in mice. *PLoS One* 3(5):e2121.
13. Heinen M, *et al.* (2012) Adult-onset fluoxetine treatment does not improve behavioral impairments and may have adverse effects on the Ts65Dn mouse model of Down syndrome. *Neural Plast* 2012:467251.
14. Burgess A, *et al.* (2010) Loss of human Greatwall results in G2 arrest and multiple mitotic defects due to deregulation of the cyclin B-Cdc2/PP2A balance. *Proc Natl Acad Sci U S A* 107(28):12564-12569.
15. Onda H, Lueck A, Marks PW, Warren HB, & Kwiatkowski DJ (1999) Tsc2(+/-) mice develop tumors in multiple sites that express gelsolin and are influenced by genetic background. *J Clin Invest* 104(6):687-695.
16. Sanz E, *et al.* (2009) Cell-type-specific isolation of ribosome-associated mRNA from complex tissues. *Proc Natl Acad Sci U S A* 106(33):13939-13944.
17. Tsien JZ, Huerta PT, & Tonegawa S (1996) The essential role of hippocampal CA1 NMDA receptor-dependent synaptic plasticity in spatial memory. *Cell* 87(7):1327-1338.
18. DePristo MA, *et al.* (2011) A framework for variation discovery and genotyping using next-generation DNA sequencing data. *Nat Genet* 43(5):491-498.
19. Callicott RJ & Womack JE (2006) Real-time PCR assay for measurement of mouse telomeres. *Comp Med* 56(1):17-22.
20. Cawthon RM (2002) Telomere measurement by quantitative PCR. *Nucleic Acids Res* 30(10):e47.

21. Dobin A, *et al.* (2013) STAR: ultrafast universal RNA-seq aligner. *Bioinformatics* 29(1):15-21.
22. Liao Y, Smyth GK, & Shi W (2014) featureCounts: an efficient general purpose program for assigning sequence reads to genomic features. *Bioinformatics* 30(7):923-930.
23. Love MI, Huber W, & Anders S (2014) Moderated estimation of fold change and dispersion for RNA-seq data with DESeq2. *Genome Biol* 15(12):550.
24. Capece V, *et al.* (2015) Oasis: online analysis of small RNA deep sequencing data. *Bioinformatics* 31(13):2205-2207.
25. Chou CH, *et al.* (2016) miRTarBase 2016: updates to the experimentally validated miRNA-target interactions database. *Nucleic Acids Res* 44(D1):D239-247.
26. Kamburov A, Stelzl U, Lehrach H, & Herwig R (2013) The ConsensusPathDB interaction database: 2013 update. *Nucleic Acids Res* 41(Database issue):D793-800.
27. Kanehisa M & Goto S (2000) KEGG: kyoto encyclopedia of genes and genomes. *Nucleic Acids Res* 28(1):27-30.
28. Ashburner M, *et al.* (2000) Gene ontology: tool for the unification of biology. The Gene Ontology Consortium. *Nat Genet* 25(1):25-29.
29. Ryan DP & Ehninger D (2014) Bison: bisulfite alignment on nodes of a cluster. *BMC Bioinformatics* 15:337.
30. Krueger F & Andrews SR (2011) Bismark: a flexible aligner and methylation caller for Bisulfite-Seq applications. *Bioinformatics* 27(11):1571-1572.
31. Halder R, *et al.* (2016) DNA methylation changes in plasticity genes accompany the formation and maintenance of memory. *Nat Neurosci* 19(1):102-110.
32. Zhang Y, *et al.* (2008) Model-based analysis of ChIP-Seq (MACS). *Genome Biol* 9(9):R137.
33. Quinlan AR & Hall IM (2010) BEDTools: a flexible suite of utilities for comparing genomic features. *Bioinformatics* 26(6):841-842.

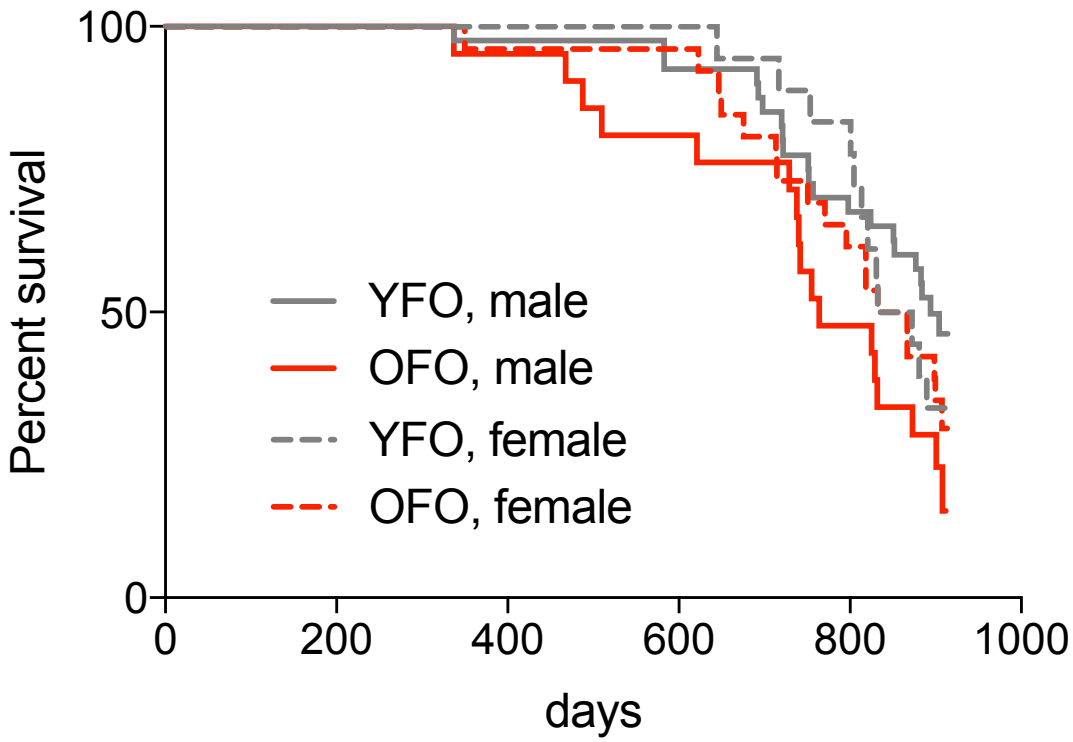

Fig. S1: **Lifespan data analyzed by paternal age and sex**. The figure shows the lifespan data presented in Fig. 1 stratified by sex (YFO male, *n* = 40 mice; OFO male, *n* = 21 mice; YFO female, *n* = 18 mice; OFO female, *n* = 26 mice). Cox proportional hazards regression revealed a significant effect of paternal age (*P* = 0.018), no measurable effect of sex (*P* = 0.47), as well as no paternal age x sex interaction (*P* = 0.20).

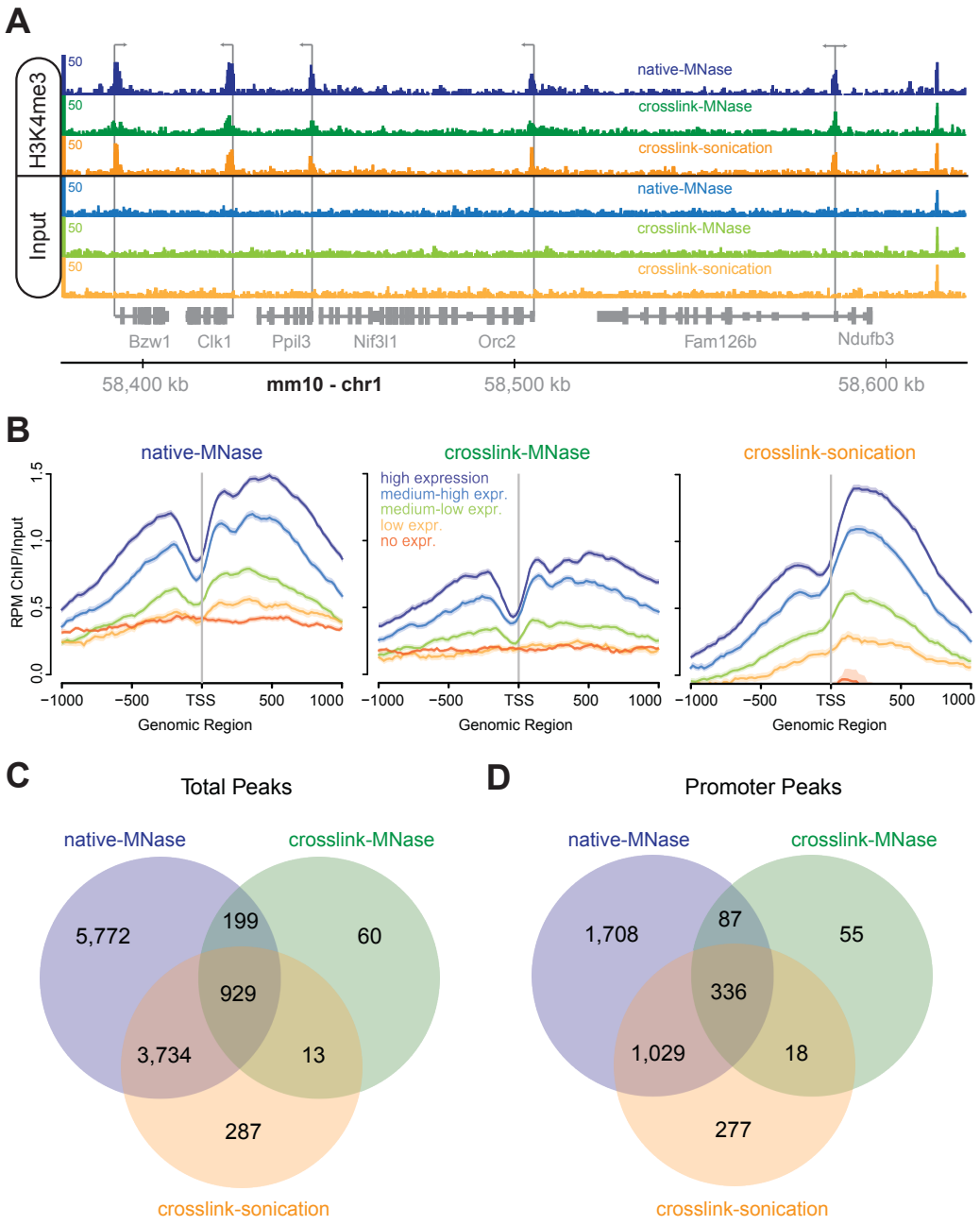

Fig. S2: **Sperm ChIP-seq optimization.** To obtain reliable information on chromatin modification changes in the sperm of old and young fathers, we first optimized the ChIP chromatin extraction protocol. We have used three different chromatin extraction protocols (see Material and Methods). In the first protocol, native chromatin was fragmented using MNase digestion (native-MNase), yielding large amounts of evenly fragmented, unfixed chromatin. A second, widely used protocol first fixes and subsequently fragments the chromatin using sonication (crosslink-sonication) that results in smaller amounts of fixed and therefore stabilized chromatin with higher size-variability. The third chromatin extraction protocol we tested fixed the chromatin and subsequently fragmented it using MNase (crosslink-MNase), yielding smaller amounts of fixed, evenly fragmented chromatin. To obtain quality information for the different protocols we performed H3K4me3 ChIP-seq experiments with the different chromatin extractions and compared the results to input chromatin. All experiments were conducted with two technical replicates. (**A**) Overall, all chromatin extraction protocols yielded H3K4me3 peaks at active gene promoters in sperm when compared to input. The crosslink-MNase protocol resulted in a notable reduction in peak size compared to the other two protocols. Transcriptional start sites of genes are denoted by arrows and genes within a 200 kb region of mouse chromosome 1 (mm10) are shown. (**B**) Aggregate H3K4me3 promoter occupancy plots for genes that are grouped into five distinct RNA expression classes (high to no expression). Aggregate gene plots for the three different chromatin extraction protocols showed strong enrichment for highly expressed genes and little enrichment for genes expressed at low levels or not expressed at all. As also shown in (**A**), H3K4me3 peak enrichment appeared to be reduced in the crosslink-MNase protocol. (**C**, **D**) Comparison of the common and distinct H3K4me3 total (**C**), as well as promoter (**D**) peaks for the three extraction protocols. Comparing all significant peaks, the native-MNase protocol detects most, the crosslink-MNase protocols the least amount of peaks, and most of the peaks of the crosslink-MNase and crosslink-sonication protocols are shared with the native-MNase protocol. When sub-setting the peak list to annotated gene promoters a general three fold reduction in peak numbers can be observed. In summary, we decided to use the native-MNase extraction protocol for all further experiments since it yielded the largest number for high-quality H3K4me3 peaks that correlated well with active gene expression.

Upstream Regulators	P value of overlap	Molecule Type	Predicted Activation
lipopolysaccharide	3.58E-18	chemical drug	Activated
TNF	4.94E-14	cytokine	
tretinoin	1.30E-13	chemical - endogenous mammalian	Activated
IFNG	2.75E-13	cytokine	Activated
IGF1	3.37E-13	growth factor	
IL6	6.62E-12	cytokine	
STAT3	4.00E-11	transcription regulator	
TGFB1	1.10E-10	growth factor	
CTNNB1	1.63E-10	transcription regulator	Activated
beta-estradiol	1.89E-09	chemical - endogenous mammalian	
E. coli B4 lipopolysaccharide	2.74E-09	chemical toxicant	
dexamethasone	3.26E-09	chemical drug	
IL1B	3.30E-09	cytokine	
WNT3A	5.64E-09	cytokine	
phorbol myristate acetate	6.21E-09	chemical drug	
TCF7L2	7.93E-09	transcription regulator	Inhibited
EGR1	9.08E-09	transcription regulator	Activated
SB203580	9.74E-09	chemical - kinase inhibitor	Inhibited
IL13	1.79E-08	cytokine	
mifepristone	2.27E-08	chemical drug	
IKBKB	3.01E-08	kinase	Activated
PD98059	4.52E-08	chemical - kinase inhibitor	
poly rI:rC-RNA	6.11E-08	biologic drug	Activated
Ifnar	7.28E-08	group	
LEP	1.12E-07	growth factor	

Top Causal Networks	P value	Predicted activation
HECW1	2.52E-18	
MIRLET7	6.19E-18	
GATA3	1.70E-17	Inhibited
Smad1/5/8-Smad4	8.76E-17	
TREM2	1.73E-16	Activated

Top Diseases and Disorders	P value
Inflammatory Response	5.63E-04 - 1.21E-11
Cancer	7.38E-04 - 8.87E-10
Organismal Injury and Abnormalities	7.38E-04 - 8.87E-10
Reproductive System Disease	5.04E-04 - 8.87E-10
Endocrine System Disorders	5.63E-04 - 1.58E-08

Top Molecular and Cellular Functions	P value
Cellular Movement	6.38E-04 - 2.00E-15
Cell-To-Cell Signaling and Interaction	7.47E-04 - 8.08E-11
Cell Morphology	6.87E-04 - 3.58E-10
Cellular Development	6.95E-04 - 8.61E-10
Cellular Growth and Proliferation	6.95E-04 - 8.61E-10

Top Physiological System Development and Function	P value
Immune Cell Trafficking	5.43E-04 - 3.50E-14
Tissue Morphology	7.10E-04 - 2.07E-13
Hematological System Development and Function	6.46E-04 - 9.28E-13
Embryonic Development	6.87E-04 - 7.54E-09
Organismal Development	7.40E-04 - 7.54E-09

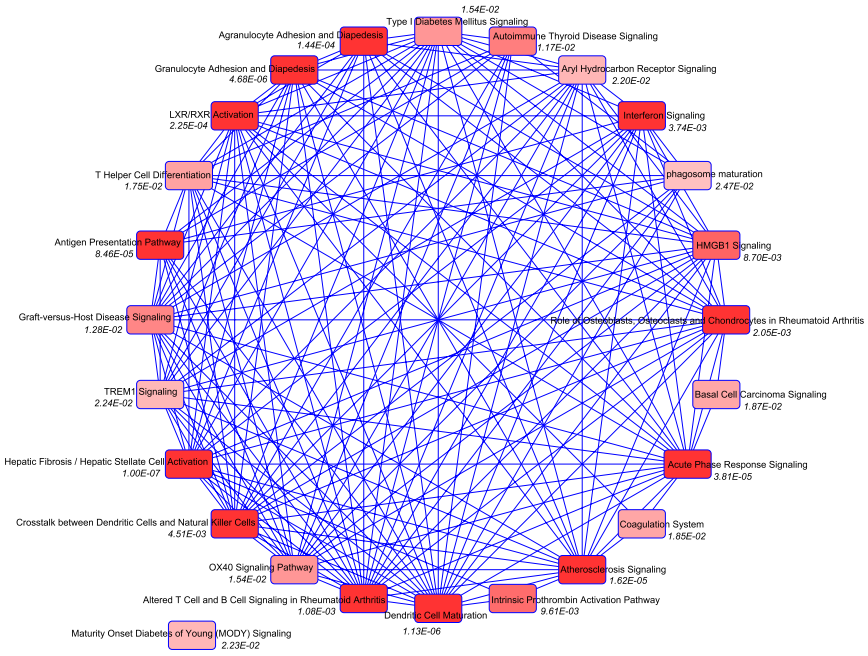

Fig. S3: **Differentially expressed genes in old father offspring tissue were enriched for immune and inflammatory regulators.** The figure shows the results of a broader pathway analysis of 720 genes ($P < 0.05$) identified in our RNA-seq study comparing old father offspring and young father offspring transcriptomes. The tables identify upstream regulators predicted to regulate genes within this gene set (*P* values indicate significance of overlap; shown is also the predicted activation state of the regulator with its gene set), top causal networks predicted to regulate these genes, top diseases and disorders, top molecular and cellular functions, as well as top physiological system development processes and functions with significant enrichment in this gene set (*P* values refer to *P* value ranges, minimal to maximal, of sub-items within the respective category). The image shows canonical pathways with significant enrichment (*P* values are shown).

Upstream Regulators	P value of overlap	Molecule Type	Predicted Activation
DYSF	4.18E-18	other	
IFNG	5.44E-15	cytokine	Activated
Ifnar	1.48E-13	group	Activated
lipopolysaccharide	2.36E-13	chemical drug	Activated
TRIM24	3.58E-13	transcription regulator	Inhibited
poly rI:rC-RNA	2.73E-11	biologic drug	Activated
IRF7	3.66E-11	transcription regulator	Activated
IFNA2	3.81E-11	cytokine	Activated
APP	1.22E-10	other	Activated
STAT1	1.39E-10	transcription regulator	Activated
methylprednisolone	2.08E-10	chemical drug	
tretinoin	4.27E-09	chemical - endogenous mammalian	Activated
TNF	1.14E-08	cytokine	Activated
TGFB1	1.79E-08	growth factor	
IL1B	1.95E-08	cytokine	Activated
IL4	2.43E-08	cytokine	Activated
KRAS	4.47E-08	enzyme	
IFN alpha/beta	4.93E-08	group	Activated
mir-21	6.56E-08	microrna	Inhibited
cholesterol	6.99E-08	chemical - endogenous mammalian	
TP53	7.78E-08	transcription regulator	Activated
Interferon alpha	1.46E-07	group	Activated
IFNB1	2.57E-07	cytokine	Activated
IRF3	3.31E-07	transcription regulator	Activated
PTGER4	4.83E-07	g-protein coupled receptor	Inhibited

Top Causal Networks	P value	Predicted activation
IFNGR2	5.73E-22	Activated
LIFR	7.88E-20	
CRLF1	8.06E-20	Activated
CLC	8.57E-20	Activated
Ifnz (includes others)	1.04E-18	Activated

Top Diseases and Disorders	P value
Endocrine System Disorders	2.25E-04 - 2.42E-13
Gastrointestinal Disease	1.88E-03 - 2.42E-13
Immunological Disease	2.03E-03 - 2.42E-13
Metabolic Disease	2.25E-04 - 2.42E-13
Cancer	1.88E-03 - 1.93E-12

Top Molecular and Cellular Functions	P value
Cellular Growth and Proliferation	7.79E-04 - 1.85E-11
Cell Death and Survival	2.03E-03 - 8.03E-11
Cellular Function and Maintenance	1.94E-03 - 6.87E-10
Cellular Movement	1.99E-03 - 8.91E-10
Cell Morphology	1.92E-03 - 1.47E-09

Top Physiological System Development and Function	P value
Organismal Survival	2.13E-04 - 7.04E-14
Hematological System Development and Function	1.99E-03 - 1.43E-09
Tissue Morphology	1.63E-03 - 1.43E-09
Immune Cell Trafficking	1.99E-03 - 1.89E-07
Organismal Development	1.83E-03 - 4.21E-07

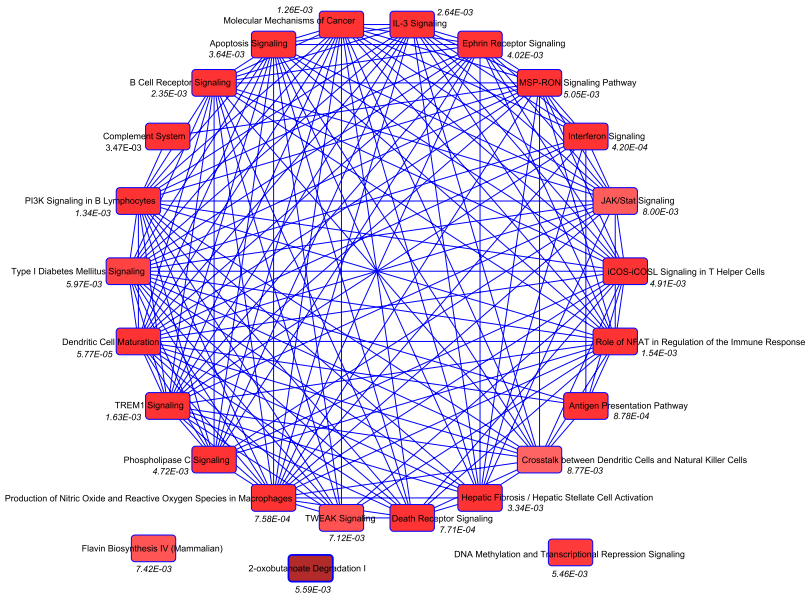

Fig. S4: **Differentially expressed genes in aged testis were enriched for immune and inflammatory regulators.** The figure shows the results of a pathway analysis of 1,985 genes ($P < 0.05$) identified in our RNA-seq study comparing transcriptomes across young and aged testes. The tables identify upstream regulators predicted to regulate genes within this gene set (*P* values indicate significance of overlap; shown is also the predicted activation state of the regulator with its gene set), top causal networks predicted to regulate these genes, top diseases and disorders, top molecular and cellular functions, as well as top physiological system development processes and functions with significant enrichment in this gene set (*P* values refer to *P* value ranges, minimal to maximal, of sub-items within the respective category). The image shows canonical pathways with significant enrichment (*P* values are shown).

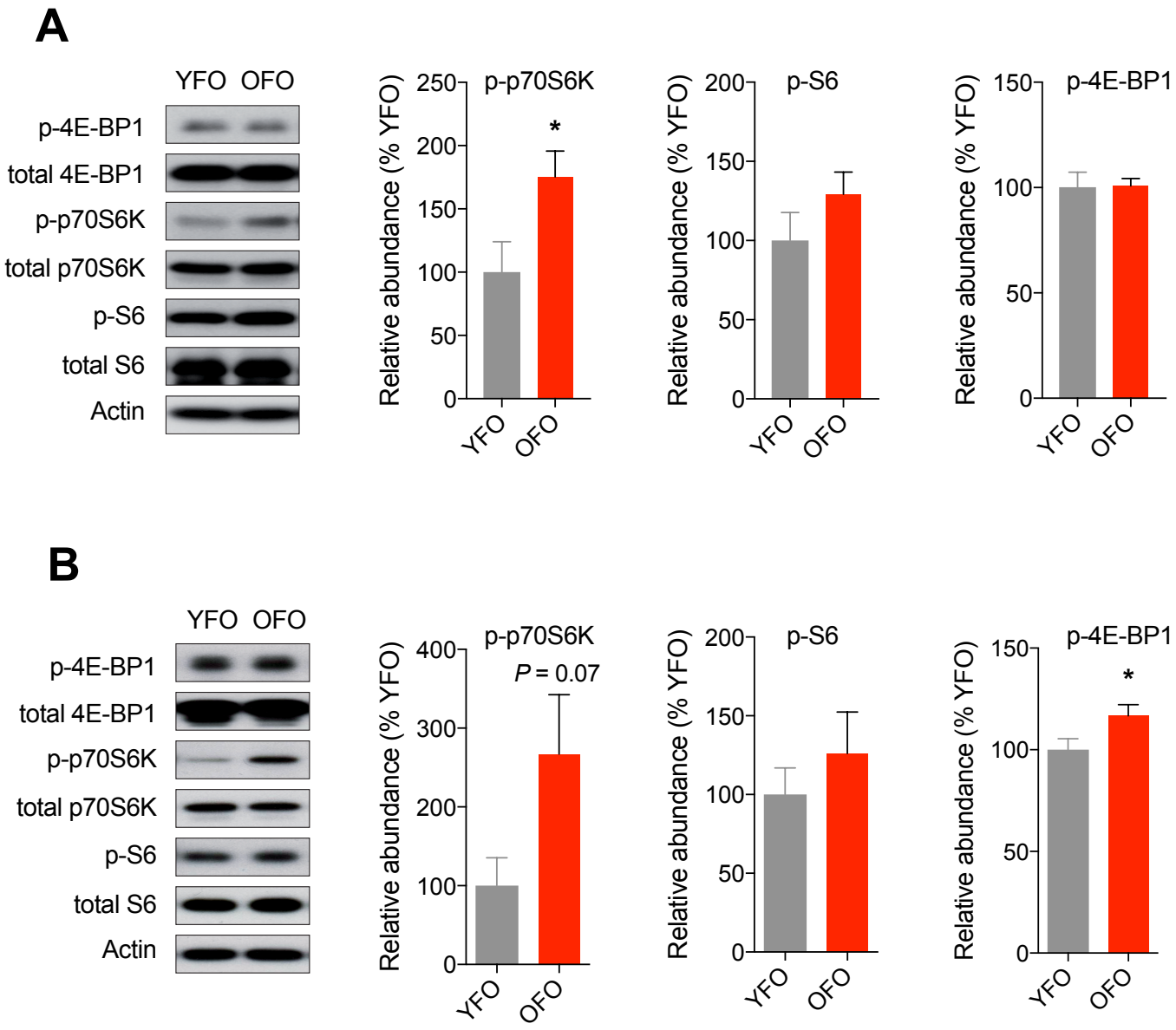

Fig. S5: **Western blot experiments provided evidence for an increased mTORC1 activation state in peripheral tissues.** (**A**) Lung. (**B**) Liver. Bar graphs show the phosphorylation status (i.e., phospho-protein normalized to total protein) of the mTORC1 downstream effectors p70S6K at Thr389 (lung: YFO, *n* = 6 mice from 6 litters; OFO, *n* = 5 mice from 5 litters; liver: *n* = 6 mice from 6 litters per group), ribosomal protein S6 at Ser240/244 (lung and liver, respectively: *n* = 6 mice from 6 litters per group), and 4E-BP1 at Thr37/46 (lung: *n* = 6 mice from 6 litters per group; liver: *n* = 12 mice from 12 litters per group). Graphs show mean +/- SEM. * $P < 0.05$.

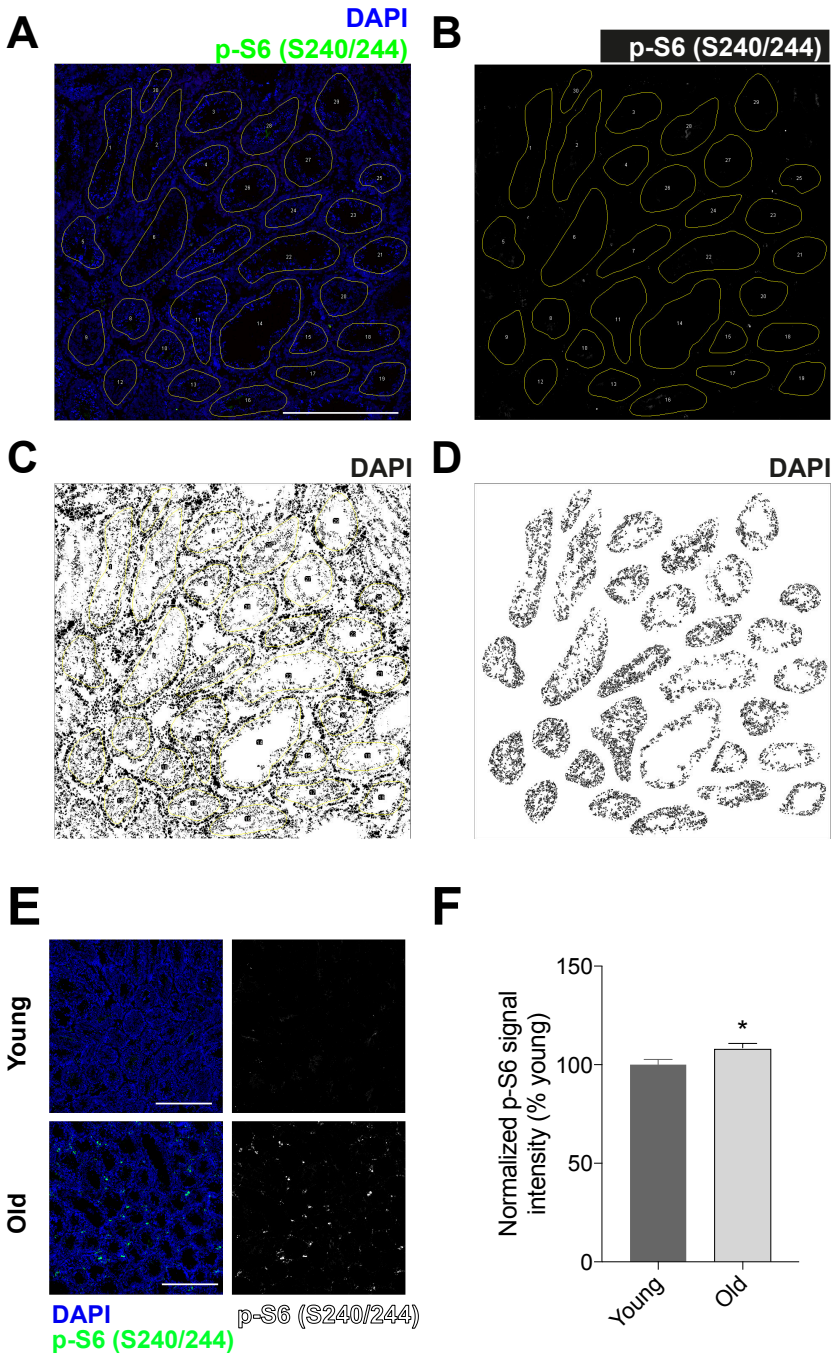

Fig. S6: **Analysis of phosphorylated S6 signal in germ cells with fluorescence intensity analysis**. Histology-based fluorescence intensity analyses were carried out to assess the phosphorylation of ribosomal protein S6 at Ser240/244 within spermatogenic cell lineages in testis derived from young (3 months old) and old (20 months old) C57BL/6J Rj mice. Tile scan Z stack maximum intensity projections were collected from immunolabeled testis sections (12 μm thick) by collecting a 6 x 6 array of 1024 x 1024 resolution confocal images (Zeiss LSM 700). (**A**) ROIs of the seminiferous tubules were made by a researcher blind to experimental condition in stitched mosaic images leaving the basal spermatogonia layer excluded from the ROI. (**B**) Then total corrected fluorescence intensity was measured from all ROIs in the p-S6 channel (488 wavelength) using the corrected total cell fluorescence method (ref. 14), taking into account background fluorescence. (**C**) Because the number of cells contained in the seminiferous tubules could bias the average intensity results, we calculated the average cell number per tubule by using the auto threshold in FIJI (ImageJ, NIH) and then applying the waterfall binary correction to differentiate profiles that contact each other, and then (**D**) obtaining a DAPI profile count only inside of the previously generated ROIs. The background corrected fluorescence was then normalized to the average cell number per tubule for that image. (**E**) Representative images of young and old testis sections. (**F**) Normalized p-S6 signals from young (n = 537 seminiferous tubules from n = 4 mice) and old (n = 335 seminiferous tubules from n = 4 mice) seminiferous tubules. * denotes $P < 0.05$. All scale bars equal 500 μm.

Upstream Regulators	P value of overlap	Molecule Type	Predicted Activation
IFNG	1.94E-53	cytokine	Inhibited
lipopolysaccharide	6.30E-49	chemical drug	Inhibited
E. coli B4 lipopolysaccharide	1.02E-42	chemical toxicant	Inhibited
Ifnar	1.64E-36	group	
IRF7	3.40E-30	transcription regulator	Activated
IL6	1.62E-29	cytokine	Inhibited
IL1B	1.64E-29	cytokine	Inhibited
TNF	2.91E-29	cytokine	Inhibited
tretinoin	7.54E-28	chemical - endogenous mammalian	Inhibited
IRF3	1.29E-27	transcription regulator	Activated
Interferon alpha	1.74E-27	group	
STAT1	3.05E-26	transcription regulator	
TRIM24	8.57E-26	transcription regulator	
poly rI:rC-RNA	1.10E-25	biologic drug	
STAT3	1.35E-25	transcription regulator	Inhibited
IL4	4.77E-23	cytokine	Inhibited
inosine	1.16E-22	chemical - endogenous mammalian	Inhibited
IL10	3.41E-22	cytokine	
SPI1	4.69E-22	transcription regulator	Inhibited
IFNB1	1.07E-21	cytokine	
IFNAR1	6.39E-21	transmembrane receptor	
IFNA2	7.86E-21	cytokine	
IL21	8.33E-21	cytokine	
DNASE2	2.23E-20	enzyme	
TGFB1	6.96E-20	growth factor	Inhibited

Top Causal Networks	P value	Predicted activation
GATA3	3.67E-53	Activated
IFNG	1.34E-51	Inhibited
lipopolysaccharide	2.08E-44	Inhibited
E.coli B4 lipopolysaccharide	6.84E-42	Inhibited
UBE3C	2.16E-38	

Top Diseases and Disorders	P value
Endocrine System Disorders	3.01E-07 - 3.55E-45
Gastrointestinal Disease	2.26E-07 - 3.55E-45
Immunological Disease	3.79E-07 - 3.55E-45
Metabolic Disease	2.99E-09 - 3.55E-45
Inflammatory Response	3.44E-07 - 5.23E-44

Top Molecular and Cellular Functions	P value
Cell-To-Cell Signaling and Interaction	3.86E-07 - 4.91E-52
Cellular Function and Maintenance	4.52E-07 - 5.25E-42
Cellular Movement	4.66E-07 - 9.06E-40
Cellular Development	3.26E-07 - 1.85E-32
Cellular Growth and Proliferation	2.49E-07 - 1.85E-32

Top Physiological System Development and Function	P value
Hematological System Development and Function	4.66E-07 - 5.66E-44
Immune Cell Trafficking	4.66E-07 - 5.66E-44
Tissue Morphology	3.79E-07 - 8.35E-32
Humoral Immune Response	3.48E-08 - 1.31E-23
Tissue Development	3.44E-07 - 2.72E-23

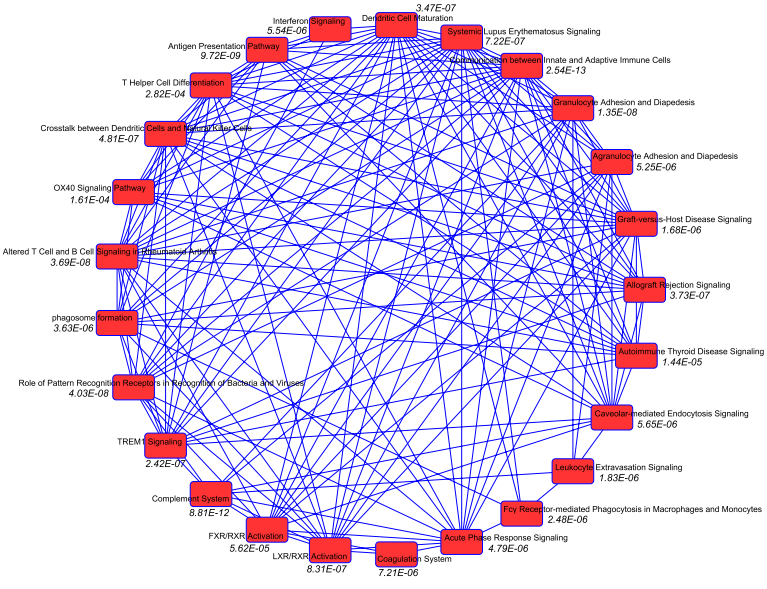

Fig. S7: **Rapamycin counteracted immune- and inflammation-related transcriptional changes associated with aging.** The figure shows the results of an Ingenuity pathway analysis focusing on a gene set differentially expressed in aged (~24 months, *n* = 2 mice) vs. young (~4 months, *n* = 2 mice) hippocampus (*n* = 402 genes; FDR < 0.1), as revealed by an RNA-seq analysis of young vs. old rapamycin or vehicle control-treated animals. Mean expression changes induced by rapamycin treatment in this gene set were used for the analysis. The tables identify upstream regulators predicted to regulate these genes (*P* values indicate significance of overlap; shown is also the predicted activation state of the regulator with its gene set), top causal networks predicted to regulate this set of genes, top diseases and disorders, top molecular and cellular functions, as well as top physiological system development processes and functions with significant enrichment among this set of differentially expressed genes (*P* values refer to *P* value ranges, minimal to maximal, of sub-items within the respective category). The image shows canonical pathways with significant enrichment (*P* values are shown).

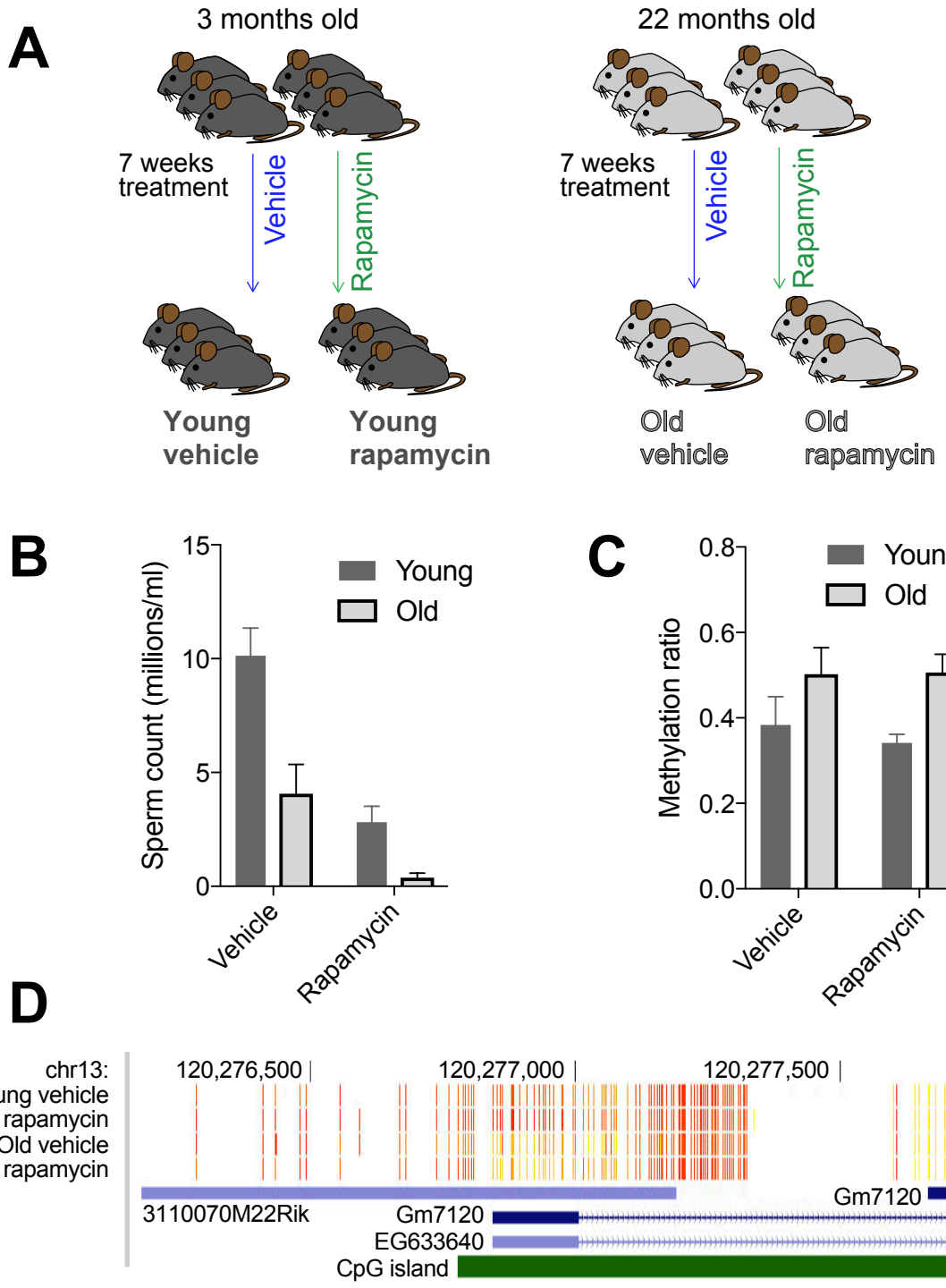

Fig. S8: **A 7-weeks rapamycin treatment regimen did not modify altered DNA methylation in sperm of aged mice.** (**A**) The schematic illustrates experimental design. (**B**) Sperm counts in epididymal swim out of young and old mice subjected to rapamycin or vehicle control (young/vehicle, young/rapamycin, old/rapamycin: *n* = 9 mice per group; old/vehicle: *n* = 5 mice). Rapamycin substantially decreased sperm counts across age groups (two-way ANOVA with the between-subjects factors age and treatment: effect of age, $P < 0.0001$; effect of treatment, $P < 0.0001$; age x treatment interaction, $P = 0.06$). (**C**, **D**) CpG methylation, examined by targeted bisulfite sequencing, of a genomic area upstream of and overlapping with *Gm7120* (chr13: 120276057-120277892; young/vehicle, young/rapamycin, old/vehicle: *n* = 5 mice per group; old/rapamycin: *n* = 4 mice). The expected aging-associated hypermethylation in this genomic area in sperm was not modified by rapamycin in any obvious way (**C**, shown are average CpG methylation ratios across this region; two-way ANOVA with the between-subjects factors age and treatment: effect of age, $P = 0.02$; effect of treatment, $P = 0.71$; age x treatment interaction, $P = 0.67$). (**D**) Representative CpG methylation tracks across this genomic area. Yellow denotes high methylation ratios, red indicates low methylation levels. Graphs show mean +/- SEM.

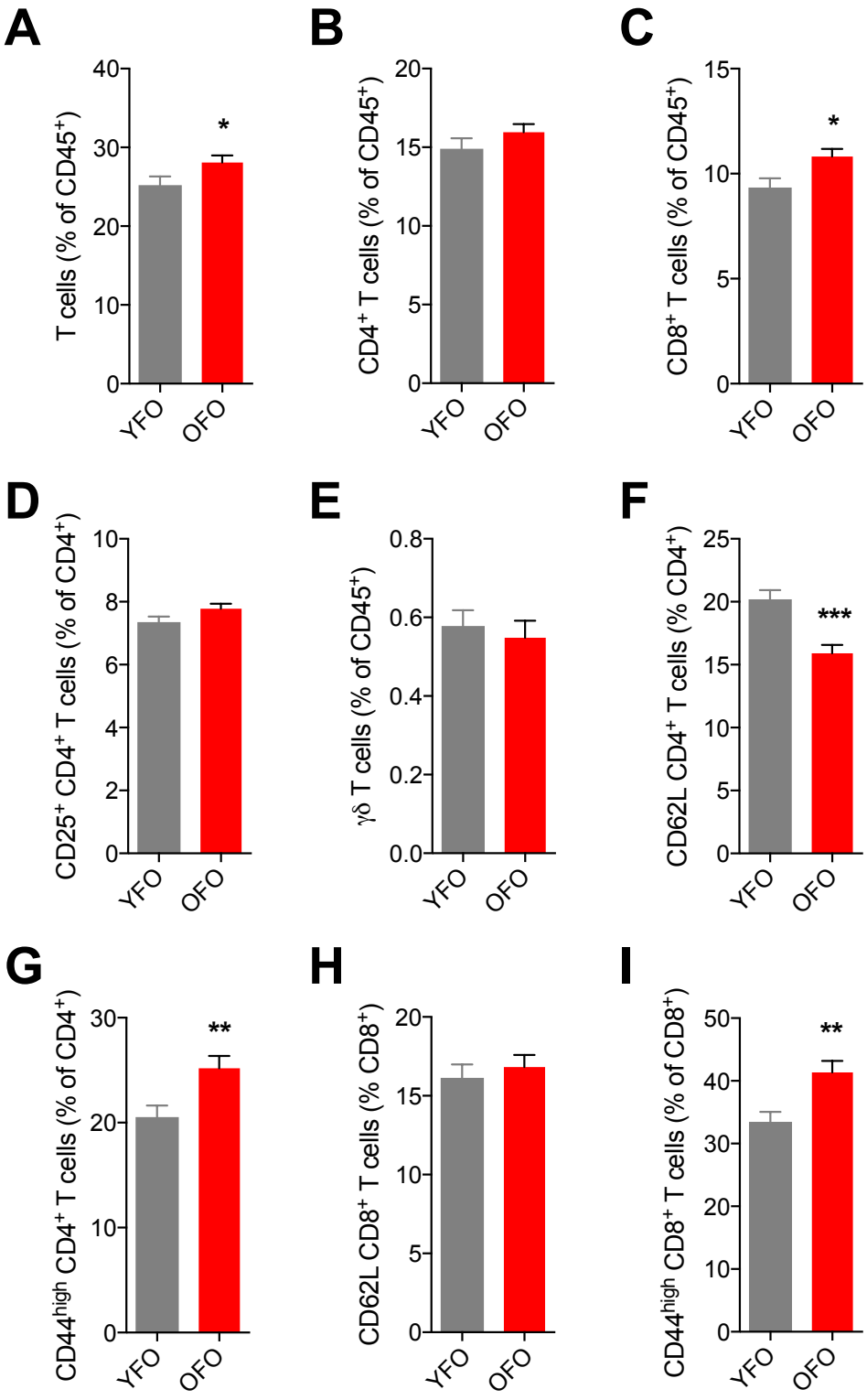

Fig. S9: **Increased abundance of CD44^{high}-expressing T cells in old father offspring mice.** Results of FACS-based quantification of peripheral blood leukocytes in young and old father offspring mice (YFO, *n* = 27 mice from 11 litters; OFO *n* = 29 mice from 10 litters). (**A**) T cells; (**B**) CD4$^+$ T cells; (**C**) CD8$^+$ T cells; (**D**) CD25$^+$ CD4$^+$ T cells; (**E**) γδ T cells; (**F**) CD62L-expressing CD4$^+$ T cells; (**G**) CD44^{high}-expressing CD4$^+$ T cells; (**H**) CD62L-expressing CD8$^+$ T cells; (**I**) CD44^{high}-expressing CD8$^+$ T cells. Graphs show mean +/- SEM. * $P < 0.05$; ** $P < 0.01$; *** $P < 0.001$.

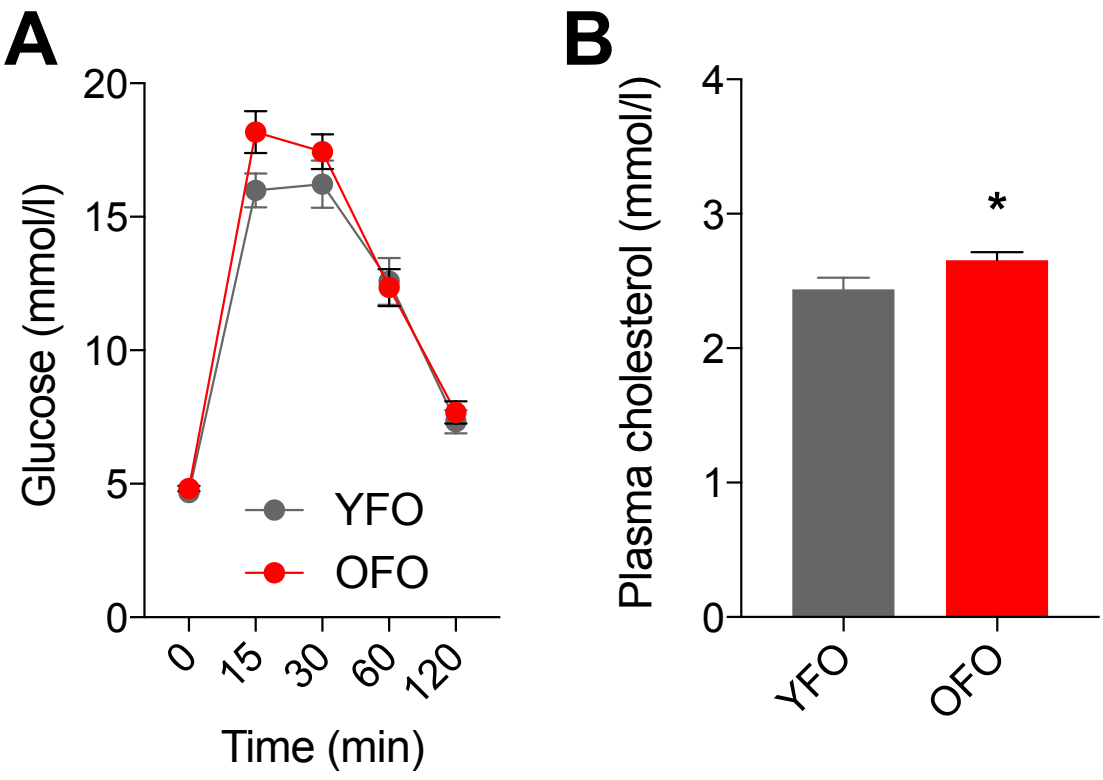

Fig. S10: **Metabolic changes in old father offspring mice.** (**A**) Plasma glucose concentrations during an intraperitoneal glucose tolerance test in young and old father offspring mice (approx. 6 months old; YFO, n = 27 mice from 11 litters; OFO, n = 29 mice from 10 litters), where time point "0 min" corresponds to plasma glucose concentrations prior to glucose bolus injection and additional time points refer to plasma glucose levels after intraperitoneal glucose injection. Two-way ANOVA with the between-subjects factor paternal age and the within-subjects factor time point revealed a significant paternal age x time interaction ($P = 0.04$; main effect of time point: $P < 0.0001$; main effect of paternal age: $P = 0.29$). (**B**) Plasma cholesterol concentrations in old and young father offspring mice (approx. 6 months old; YFO, n = 27 mice from 11 litters; OFO, n = 29 mice from 10 litters). Graphs show mean +/- SEM. * $P < 0.05$.

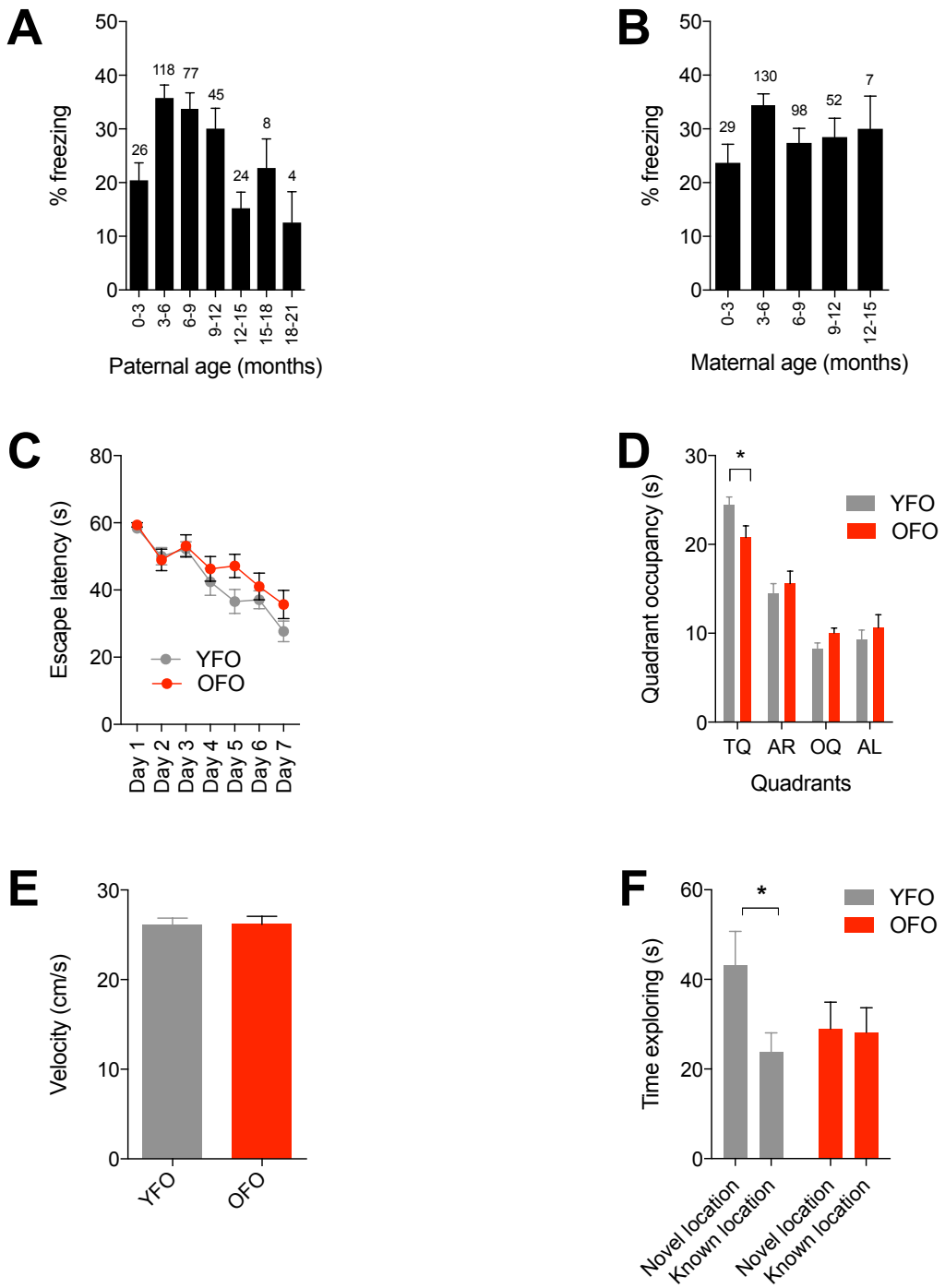

Fig. S11: **Advanced paternal age effects on learning and memory**. (**A**) Stratification of a large fear conditioning dataset by paternal age revealed an inverted U-shaped relationship of paternal age and freezing behavior in offspring mice (ANOVA, effect of paternal age, P = 0.0008). Numbers of animals within each paternal age bin are reported in the figure. (**B**) Stratification of this fear conditioning dataset by maternal age did not reveal a significant effect of maternal age (ANOVA, effect of maternal age, P = 0.14). (**C**) – (**F**) Spatial learning in young and old father offspring animals was tested in a hidden version of the Morris water maze ((**C**) – (**E**); YFO, n = 25 mice from 10 litters; OFO, n = 17 mice from 7 litters) and in an object-place-recognition paradigm, respectively ((**F**); YFO, n = 16 mice from 6 litters; OFO, n = 14 mice from 6 litters). (**C**) Escape latencies during training trials in the Morris water maze (ANOVA, effect of training day, P < 0.0001; effect of paternal age, P = 0.11; interaction paternal age x training day, P = 0.40). (**D**) Quadrant occupancies of young and old father offspring during probe trial assessment in the Morris water maze (ANOVA, effect of quadrant, P < 0.0001; effect of paternal age, P = 0.67; interaction paternal age x quadrant, P = 0.10; planned comparison by unpaired t-test, target occupancy YFO vs. OFO, P = 0.02); TQ – target quadrant, AR – adjacent right quadrant, OQ – opposite quadrant, AL – adjacent left quadrant. (**E**) Swim speed during probe trial assessment did not differ measurably between YFO and OFO mice (unpaired t-test, P = 0.96). (**F**) Testing young and old father offspring animals in an object place recognition learning paradigm showed that exploration times in young father offspring were significantly higher for an object in a novel location than for an object in a known location, while exploration times in old father offspring did not differ between the object in the known location and the object in the novel location (ANOVA, effect of object location, P = 0.0064; effect of paternal age, P = 0.53; interaction paternal age x object location, P = 0.01; planned comparison by unpaired t-test, novel location vs. known location: YFO, P = 0.03; OFO, P = 0.93). Graphs show means +/- SEM. * denotes P < 0.05.

Chromosome	Start	End	Gene Symbol	UCSC ID	Distance (bp)	Methylation difference	P value	FDR
					to TSS	old-young		
chr1	113761495	113763495	Dsel	uc007chy.1	0	-0.0625	0	0
chr10	23868122	23870122	Stx7	uc007eqs.1	0	-0.125	0	0
chr11	11585215	11587215	Ikzf1	uc007iaj.1	0	-0.022869	0	0
chr11	80191517	80193517	5730455P16Rik	uc007klv.2	0	-0.12	0	0
chr13	21872423	21874423	Hist1h3h	uc007prc.1	843	-0.058824	0	0
chr13	21872423	21874423	Hist1h1b	uc007pri.1	0	-0.058824	0	0
chr13	120275845	120277845	Gm7120	uc007rzl.1	0	0.07144	0	0
chr13	120275845	120277845	EG633640	uc007rzm.1	0	0.07144	0	0
chr13	120276666	120278666	3110070M22Rik	uc007rzk.2	0	0.07067	0	0
chr13	120276666	120278666	Gm7120	uc007rzl.1	0	0.07067	0	0
chr13	120276666	120278666	EG633640	uc007rzm.1	0	0.07067	0	0
chr13	120277191	120279191	3110070M22Rik	uc007rzk.2	0	0.08255	0	0
chr13	120277191	120279191	Gm7120	uc007rzl.1	345	0.08255	0	0
chr13	120277191	120279191	EG633640	uc007rzm.1	345	0.08255	0	0
chr13	120277191	120279191	3110070M22Rik	uc007rzk.2	0	0.08255	0	0
chr13	120277191	120279191	EG633640	uc007rzm.1	345	0.08255	0	0
chr2	127657595	127659595	Bub1	uc008mge.2	0	-0.041667	0	0
chr2	163996849	163998849	Kcns1	uc008ntv.1	0	0.051282	0	0
chr5	23536501	23538501	Fam126a	uc008wqu.1	-371	-0.166667	0	0
chr5	137927044	137929044	Epo	uc009acm.1	0	0.021277	0	0
chr5	139936488	139938488	3110082I17Rik	uc009agk.1	0	0.033333	0	0
chr8	4275905	4277905	Timm44	uc009ktq.2	0	-0.138889	0	0
chr8	108375908	108377908	Cenpt	uc009nef.1	0	-0.033333	0	0
chrX	50973585	50975585	Cxx1a	uc009tfe.2	0	0.037037	0	0
chrX	70458703	70460703	Xlr4b	uc009tlj.1	0	0.142857	0	0
chrX	86004892	86006892	Mir1906-1	uc012hlo.1	0	0.1	0	0
chrX	132162244	132164244	Prame	uc012hos.1	0	0.181818	0	0
chrX	156576268	156578268	Pdha1	uc009utc.1	0	0.090909	0	0
chr16	31947631	31949631	0610012G03Rik	uc007yxy.2	0	-0.016665	0	0.000002
chr16	31947631	31949631	Ncbp2	uc007yxz.2	0	-0.016665	0	0.000002
chr10	12809593	12811593	Plagl1	uc011xag.1	0	0.030228	0	0.000008
chr10	12809593	12811593	Zac1	uc007ekn.1	0	0.030228	0	0.000008
chr3	40602872	40604872	Plk4	uc008pbm.1	0	-0.041758	0	0.000071
chr1	120207709	120209709	Tsn	uc007cib.1	0	0.033468	0	0.000075
chr11	87429665	87431665	Hsf5	uc007kuc.1	0	0.04402	0	0.000121
chr2	69484311	69486311	Bbs5	uc008jyf.1	0	-0.077077	0	0.000121
chr19	38128514	38130514	AK153534	uc008hiw.1	0	-0.039873	0	0.000176
chr19	38128514	38130514	Cep55	uc008hix.2	0	-0.039873	0	0.000176
chr19	38128531	38130531	AK153534	uc008hiw.1	0	-0.039873	0	0.000176
chr19	38128531	38130531	Cep55	uc008hix.2	0	-0.039873	0	0.000176
chr5	145305755	145307755	Nptx2	uc012egq.1	0	0.024269	0	0.00021
chr5	72950884	72952884	Nfxl1	uc008xrl.1	0	-0.066512	0.000001	0.000383
chr10	110942341	110944341	Phlda1	uc007haf.2	0	-0.029212	0.000001	0.000413
chr4	88418897	88420897	Gm13285	uc008tnn.2	0	0.068046	0.000001	0.000413
chr1	36592574	36594574	Ankrd23	uc007aql.1	0	-0.026657	0.000001	0.000476
chr4	88429957	88431957	Gm13285	uc008tnn.2	-1924	0.096686	0.000001	0.000603
chr4	88429957	88431957	Gm13276	uc008tnq.2	0	0.096686	0.000001	0.000603
chr17	35959301	35961301	Ier3	uc008cio.1	643	-0.060355	0.000002	0.000674
chr17	35959301	35961301	Flot1	uc008cip.1	0	-0.060355	0.000002	0.000674
chr5	110714337	110716337	Pxmp2	uc008yqj.1	0	-0.018705	0.000002	0.000675

Table S1: **Reduced representation bisulfite sequencing (RRBS) revealed a broad set of differentially methylated promoters in old sperm**. RRBS analyses of sperm from young (4 months old) vs. aged (24 months old) mice (pooling equimolar amounts of DNA of n = 5 mice per group) identified promoters differentially methylated in sperm as a consequence of aging. The table shows the top of the list of genes with differentially methylated promoters. Shown are genomic coordinates, gene IDs, methylation differences (old – young), P values and false discovery rates (FDR).

Upstream Regulators	P value of overlap	Molecule Type	Predicted Activation
TP53	3.44E-12	transcription regulator	
RAD21	5.91E-10	transcription regulator	
CTCF	9.54E-08	transcription regulator	
CDKN1A	1.19E-07	kinase	
FOS	1.54E-07	transcription regulator	
HNF4A	1.80E-07	transcription regulator	
MYC	2.12E-07	transcription regulator	
beta-estradiol	6.52E-07	chemical - endogenous mammalian	
tretinoin	8.09E-07	chemical - endogenous mammalian	Activated
trichostatin A	1.53E-06	chemical drug	Activated
5-azacytidine	2.84E-06	chemical drug	Activated
CTNNB1	3.26E-06	transcription regulator	
L-dopa	6.42E-06	chemical - endogenous mammalian	
TGFB1	9.27E-06	growth factor	
HTT	1.18E-05	transcription regulator	
MYCN	1.40E-05	transcription regulator	
miR-26a-5p (and other miRNAs w/seed UCAAGUA)	1.49E-05	mature microrna	
ESR1	1.65E-05	ligand-dependent nuclear receptor	
gentamicin	1.92E-05	chemical drug	
IGF1	2.27E-05	growth factor	
miR-124-3p (and other miRNAs w/seed AAGGCAC)	2.85E-05	mature microrna	
GnRH analog	3.95E-05	biologic drug	
UCN-01	4.42E-05	chemical drug	
ELAVL1	5.45E-05	other	
NRG1	7.16E-05	growth factor	

Top Causal Networks	P value	Predicted activation
EP300	3.25E-12	
MAPK12	1.60E-11	
BUB3	4.07E-11	
SYVN1	5.38E-11	
RPS6KB1	7.22E-11	

Top Diseases and Disorders	P value
Cancer	1.14E-02 - 8.62E-19
Organismal Injury and Abnormalities	1.15E-02 - 8.62E-19
Gastrointestinal Disease	9.65E-03 - 3.60E-17
Reproductive System Disease	1.14E-02 - 2.64E-11
Developmental Disorder	1.01E-02 - 2.64E-11

Top Molecular and Cellular Functions	P value
Gene Expression	4.06E-03 - 4.32E-15
Cellular Growth and Proliferation	4.31E-03 - 7.85E-10
Cellular Development	4.14E-03 - 5.40E-09
Cell Death and Survival	4.14E-03 - 4.54E-08
Cell Morphology	4.40E-03 - 9.72E-08

Table S2: **Pathways, regulators and processes enriched in the gene set with differentially methylated promoters in aged sperm.** The tables show the results of a pathway analysis focusing on the gene set with differentially methylated promoters in old father offspring tissue ($P < 0.05$). They identify upstream regulators predicted to regulate genes with differentially methylated promoters (*P* values indicate significance of overlap; shown is also the predicted activation state of the regulator with its gene set), top causal networks predicted to regulate genes with differentially methylated promoters, top diseases and disorders, top molecular and cellular functions, as well as top physiological system development processes and functions with significant enrichment among differentially methylated promoters in aged sperm (*P* values refer to *P* value ranges, minimal to maximal, of sub-items within the respective category).

Diseases and Biological Functions	F0 sperm	F1 hippocampus
	old vs. Young	OFO vs. YFO
organismal death	-4.89	-8.35
perinatal death	-1.64	-4.28
organization of cytoskeleton	1.48	3.69
organization of cytoplasm	1.47	3.69
microtubule dynamics	1.63	3.74
proliferation of cells	1.67	3.27
proliferation of tumor cell lines	1.20	2.02
Growth Failure	-1.38	-3.73
size of embryo	1.16	3.94
cell viability	0.62	3.74
cell survival	0.86	3.89
Hypoplasia	-1.24	-3.99
formation of cellular protrusions	0.47	3.61
damage of muscle	-2.35	-1.30
dysgenesis	-1.09	-3.89
expression of RNA	1.64	2.52
neuronal cell death	-1.21	2.93
hypoplasia of organ	-1.19	-3.59
transcription	1.20	2.92
cell viability of tumor cell lines	0.85	3.01
phosphorylation of protein	1.67	2.84
size of body	2.49	0.00
apoptosis	-1.50	-2.23
quantity of cells	1.13	2.79
transcription of RNA	1.36	2.34
metabolism of protein	1.95	0.52
activation of DNA endogenous promoter	1.29	1.66
transcription of DNA	1.06	1.83
development of central nervous system	1.96	1.94
congenital anomaly of cardiovascular system	1.01	-2.88
mass of testis	-1.64	0.00
incidence of tumor	0.00	-1.98
dyspnea	0.00	-3.53
differentiation of cells	-0.32	2.72
neonatal death	-1.42	0.00
tumorigenesis of tissue	-1.14	-0.92
epithelial cancer	-1.33	-0.73
craniofacial abnormality	0.80	-2.28
malignant solid tumor	-1.71	-0.53
development of neurons	0.26	3.02
congenital anomaly of digestive system	0.00	-2.16
differentiation of bone	0.00	2.32
development of cardiovascular system	0.00	3.20
abdominal neoplasm	-0.09	-1.66
abdominal cancer	-0.27	-1.54
congenital anomaly of mouth	0.00	-2.07
micrognathia	1.32	-1.84
cell death	-1.71	-0.81
migration of embryonic cells	3.10	0.00
quantity of filaments	0.00	-3.05

Table S3: **Ingenuity pathway analyses identified diseases and biological functions associated with genes with differentially methylated promoters in F0 sperm and F1 offspring tissue.** The table shows diseases and biological functions associated with genes with differentially methylated promoters in F0 sperm (young vs. old) and F1 hippocampal tissue (young father offspring vs. old father offspring). Positive z-scores indicate activating effects, while negative z-scores imply inhibitory action on the corresponding biological process. Z-scores >2 or <-2 are considered significant.

mature	structure	chromosome	start	stop	strand	log2FoldChange	pvalue	padj
mmu-miR-411-5p	miRNA	chr12	109710190	109710210	+	-2.21	5.03E-24	5.19E-20
mmu-miR-434-5p	miRNA	chr12	109594528	109594549	+	-2.04	2.07E-17	1.07E-13
mmu_piR_039057	piRNA	Multiple	Multiple	Multiple	Multiple	-1.63	2.07E-15	5.34E-12
mmu-miR-410-3p	miRNA	chr12	109743764	109743784	+	-2.01	2.03E-15	5.34E-12
mmu-miR-541-5p	miRNA	chr12	109742422	109742446	+	-1.42	8.06E-15	1.66E-11
mmu-miR-127-3p	miRNA	chr12	109592888	109592909	+	-1.81	1.62E-13	2.78E-10
mmu-miR-434-3p	miRNA	chr12	109594565	109594586	+	-1.53	6.39E-13	9.43E-10
mmu-miR-409-3p	miRNA	chr12	109743204	109743225	+	-1.86	2.72E-12	3.50E-09
mmu-miR-431-5p	miRNA	chr12	109590459	109590479	+	-2.22	5.70E-11	6.53E-08
mmu-miR-22-3p	miRNA	chr11	75463772	75463793	+	-1.35	1.62E-10	1.67E-07
mmu-miR-880-3p	miRNA	chrX	66800540	66800561	-	-1.84	2.14E-10	2.01E-07
mmu-miR-463-5p	miRNA	chrX	66799273	66799294	-	-1.60	2.96E-10	2.35E-07
mmu-miR-883a-3p	miRNA	chrX	66780768	66780789	-	-1.70	2.93E-10	2.35E-07
mmu-miR-134-5p	miRNA	chr12	109734145	109734166	+	-1.80	7.13E-10	5.25E-07
mmu-miR-465b-5p	miRNA	chrX	66835811	66835832	-	-1.82	8.77E-10	6.03E-07
mmu_piR_018780	piRNA	Multiple	Multiple	Multiple	Multiple	-1.73	1.44E-09	7.79E-07
mmu-miR-351-5p	miRNA	chrX	53053315	53053338	-	-1.60	1.40E-09	7.79E-07
mmu-miR-465c-5p	miRNA	chrX	66832566	66832587	-	-1.60	1.39E-09	7.79E-07
mmu-miR-181c-5p	miRNA	chr8	84178924	84178945	-	-1.21	1.35E-09	7.79E-07
mmu-miR-878-5p	miRNA	chrX	66801554	66801575	-	-1.66	2.56E-09	1.20E-06
mmu-miR-101b-3p	miRNA	chr19	29135338	29135356	+	-1.62	2.56E-09	1.20E-06
mmu_piR_016952	piRNA	Multiple	Multiple	Multiple	Multiple	-1.43	2.47E-09	1.20E-06
mmu-miR-743a-3p	miRNA	chrX	66776760	66776781	-	-1.64	3.94E-09	1.77E-06
mmu_piR_003570	piRNA	Multiple	Multiple	Multiple	Multiple	-1.29	4.28E-09	1.84E-06
mmu-miR-106b-3p	miRNA	chr5	138165746	138165767	-	-1.28	6.21E-09	2.56E-06
mmu-miR-34c-3p	miRNA	chr9	51103044	51103065	-	-1.81	6.98E-09	2.77E-06
mmu-miR-145a-3p	miRNA	chr18	61647827	61647848	-	-1.34	7.41E-09	2.83E-06
mmu-miR-872-5p	miRNA	chr4	94665167	94665187	+	-1.62	8.11E-09	2.89E-06
mmu-miR-871-5p	miRNA	chrX	66810472	66810494	-	-1.42	7.92E-09	2.89E-06
mmu-miR-381-3p	miRNA	chr12	109726870	109726891	+	-2.05	8.66E-09	2.98E-06
mmu-miR-19b-3p	miRNA	chr14	115044358	115044380	+	-1.83	9.56E-09	3.18E-06
mmu-miR-881-3p	miRNA	chrX	66801954	66801975	-	-1.91	1.00E-08	3.23E-06
mmu-miR-148b-3p	miRNA	chr15	103285185	103285206	+	-1.54	1.05E-08	3.30E-06
mmu_piR_012562	piRNA	Multiple	Multiple	Multiple	Multiple	0.97	1.91E-08	5.80E-06
mmu-miR-25-3p	miRNA	chr5	138165332	138165353	-	-1.40	2.46E-08	7.24E-06
Snord47	snoRNA	chr1	161038082	161038158	+	-1.44	2.72E-08	7.79E-06
mmu-miR-3963	miRNA	chr3	151023839	151023857	-	-1.33	3.49E-08	9.48E-06
mmu-miR-741-3p	miRNA	chrX	66796809	66796831	-	-1.44	3.42E-08	9.48E-06
mmu-miR-143-3p	miRNA	chr18	61649199	61649219	-	-1.44	4.92E-08	1.30E-05
mmu_piR_002118	piRNA	Multiple	Multiple	Multiple	Multiple	-1.18	5.15E-08	1.33E-05
mmu-miR-337-5p	miRNA	chr12	109585818	109585839	+	-2.15	5.55E-08	1.33E-05
mmu-miR-34b-5p	miRNA	chr9	51103610	51103632	-	-1.57	5.45E-08	1.33E-05
mmu_piR_011982	piRNA	Multiple	Multiple	Multiple	Multiple	-1.42	5.37E-08	1.33E-05
mmu_piR_017770	piRNA	Multiple	Multiple	Multiple	Multiple	0.85	5.88E-08	1.35E-05
mmu-miR-374b-5p	miRNA	chrX	103573112	103573133	-	-1.34	5.76E-08	1.35E-05
mmu-miR-375-3p	miRNA	chr1	74900661	74900682	-	-1.27	6.76E-08	1.48E-05
mmu_piR_005971	piRNA	Multiple	Multiple	Multiple	Multiple	-1.25	6.75E-08	1.48E-05
mmu-miR-331-3p	miRNA	chr10	93963783	93963803	-	-1.78	8.29E-08	1.74E-05
mmu_piR_019332	piRNA	Multiple	Multiple	Multiple	Multiple	-2.07	8.23E-08	1.74E-05
mmu-miR-296-5p	miRNA	chr2	174267093	174267113	-	-1.52	9.15E-08	1.89E-05

Table S4: Differentially expressed sRNAs in aged sperm. The table shows the top differentially expressed sRNAs in aged sperm (aged: 22 months old, *n* = 3 mice; young: 3 months old, *n* = 8 mice).

Pathway	Source	*P* value	FDR
Insulin Signaling	Wikipathways	2.45E-08	1.58E-05
IL4-mediated signaling events	PID	3.81E-08	1.58E-05
Regulation of toll-like receptor signaling pathway	Wikipathways	6.08E-08	1.68E-05
Toll-like receptor signaling pathway	Wikipathways	1.87E-07	3.89E-05
Toll-like receptor signaling pathway - Homo sapiens (human)	KEGG	2.70E-07	4.48E-05
mTOR signaling pathway	PID	5.06E-07	6.77E-05
Oncostatin M Signaling Pathway	Wikipathways	5.71E-07	6.77E-05
il-2 receptor beta chain in t cell activation	BioCarta	9.20E-07	9.40E-05
Prolactin	NetPath	1.02E-06	9.40E-05
S1P1 pathway	PID	1.64E-06	0.00012573
Prolactin Signaling Pathway	Wikipathways	1.93E-06	0.00012573
IL-4 Signaling Pathway	Wikipathways	2.09E-06	0.00012573

Pathway	Source	*P* value	FDR
EGFR1	NetPath	7.78E-25	2.44E-21
Pathways in cancer - Homo sapiens (human)	KEGG	1.52E-23	2.38E-20
Developmental Biology	Reactome	1.49E-20	1.56E-17
Proteoglycans in cancer - Homo sapiens (human)	KEGG	2.96E-20	2.32E-17
Integrated Pancreatic Cancer Pathway	Wikipathways	2.26E-18	1.42E-15
Axon guidance	Reactome	3.47E-17	1.81E-14
TGF beta Signaling Pathway	Wikipathways	6.20E-17	2.78E-14
EGF-EGFR Signaling Pathway	Wikipathways	1.32E-16	5.18E-14
BDNF signaling pathway	Wikipathways	6.72E-16	2.24E-13
PDGFR-beta signaling pathway	PID	7.14E-16	2.24E-13
Signalling by NGF	Reactome	9.48E-16	2.71E-13
Colorectal cancer - Homo sapiens (human)	KEGG	4.52E-15	1.18E-12

Table S5: High confidence validated targets of miRNAs altered in aged sperm were significantly enriched for signaling pathways, including the mTOR pathway, insulin and growth factor signaling. The table shows the top signficantly enriched pathways among high confidence validated targets of miRNAs altered in aged sperm. The column 'source' indicates which database contains the enriched pathway. Pathway analysis was performed for miRNAs upregulated (top), as well as for miRNAs downregulated in aged sperm (bottom). The mTOR pathway was significantly enriched among targets of both up- and downregulated miRNAs.

Chr	Start	End	Strand	Annotation	Distance to TSS	Gene Name	Gene Type
chr11	108315846	108317452	+	intron (NM_011101, intron 2 of 16)	27239	Prkca	protein-coding
chr14	69390433	69392555	+	Intergenic	54343	Entpd4	protein-coding
chr5	15533225	15534327	+	Intergenic	-85323	Speer4d	protein-coding
chr5	15006992	15008114	+	Intergenic	25454	Gm17019	protein-coding
chr5	15480147	15481412	+	Intergenic	-138320	Speer4d	protein-coding
chr5	14921259	14921951	+	Intergenic	-6716	Gm9758	protein-coding
chr5	15707839	15709391	+	TTS (NM_001281511)	5656	Speer4c	protein-coding
chr5	15529370	15530033	+	Intergenic	-89398	Speer4d	protein-coding
chr5	17468164	17469367	+	Intergenic	-7357	Speer4f	protein-coding
chr5	14952929	14953807	+	intron (NR_001584, intron 1 of 3)	8074	Speer8-ps1	pseudo
chr5	15471843	15474397	+	Intergenic	-145979	Speer4d	protein-coding
chr5	14931454	14933591	+	Intergenic	5953	Speer4e	protein-coding
chr5	15702965	15703956	+	intron (NR_001585, intron 2 of 4)	10811	Speer4c	protein-coding
chr5	14933832	14934705	+	intron (NM_001122661, intron 4 of 4)	4207	Speer4e	protein-coding
chr5	14985308	14987004	+	Intergenic	-7257	Gm10354	protein-coding
chr5	14935166	14936321	+	exon (NM_001122661, exon 3 of 5)	2732	Speer4e	protein-coding
chr5	15691978	15692817	+	intron (NR_001585, intron 1 of 4)	11687	Speer7-ps1	pseudo
chr5	15645958	15647031	+	Intergenic	10565	4930572O03Rik	pseudo
chr5	14908044	14909993	+	Intergenic	5871	Gm9758	protein-coding
chr5	15468061	15468760	+	Intergenic	-150689	Speer4d	protein-coding
chr5	15656813	15657836	+	promoter-TSS (NR_073011)	-265	4930572O03Rik	pseudo
chr5	15612209	15612938	+	Intergenic	-6526	Speer4d	protein-coding
chr5	15461916	15463382	+	Intergenic	-156450	Speer4d	protein-coding
chr5	14910981	14912706	+	intron (NM_198666, intron 3 of 4)	3046	Gm9758	protein-coding
chr5	15030056	15030902	+	intron (NM_182957, intron 3 of 4)	2528	Gm17019	protein-coding
chr5	14978634	14979514	+	promoter-TSS (NM_001281514)	-175	Gm10354	protein-coding
chr5	14919467	14920164	+	Intergenic	-4926	Gm9758	protein-coding
chr5	15483068	15484798	+	Intergenic	-135166	Speer4d	protein-coding
chr5	15661254	15662025	+	Intergenic	-4580	4930572O03Rik	pseudo
chr5	15620258	15623504	+	intron (NM_025759, intron 3 of 4)	2782	Speer4d	protein-coding
chr5	14918167	14919372	+	Intergenic	-3880	Gm9758	protein-coding
chr5	14923325	14923966	+	Intergenic	-8756	Gm9758	protein-coding
chr5	15004600	15005436	+	Intergenic	-26119	Gm10354	protein-coding
chr5	14946800	14947492	+	intron (NR_001584, intron 1 of 3)	1852	Speer8-ps1	pseudo
chr5	15026911	15028590	+	Intergenic	5257	Gm17019	protein-coding
chr5	15524608	15525296	+	Intergenic	-94147	Speer4d	protein-coding
chr5	15710193	15712138	+	intron (NR_001585, intron 4 of 4)	3106	Speer4c	protein-coding
chr5	14974737	14976920	+	intron (NR_001584, intron 3 of 3)	3071	Gm10354	protein-coding
chr5	15574571	15575556	+	Intergenic	-44036	Speer4d	protein-coding
chr5	15652178	15653068	+	non-coding (NR_073011, exon 5 of 5)	4436	4930572O03Rik	pseudo
chr5	15469441	15470753	+	Intergenic	-149002	Speer4d	protein-coding
chr5	15040113	15041098	+	Intergenic	-7598	Gm17019	protein-coding
chr5	15614150	15615242	+	Intergenic	-4403	Speer4d	protein-coding
chr5	14904568	14905452	+	Intergenic	9879	Gm9758	protein-coding
chr5	15650648	15652107	+	TTS (NR_073011)	5682	4930572O03Rik	pseudo
chr5	15579201	15582115	+	Intergenic	-38441	Speer4d	protein-coding
chr5	15624853	15625868	+	Intergenic	6261	Speer4d	protein-coding
chr5	15653636	15655054	+	non-coding (NR_073011, exon 3 of 5)	2714	4930572O03Rik	pseudo
chr7	140126017	140127240	+	exon (NM_153783, exon 2 of 7)	943	Paox	protein-coding
chr7	43654939	43656003	+	intron (NM_031181, intron 6 of 6)	4690	Siglece	protein-coding
chr9	121929039	121932281	+	Intergenic	-6615	1700048O20Rik	ncRNA

Table S6: **ChIP-seq (H3K27me3) identified a hotspot for differentially occupied regions on chromosome 5 in aging sperm.** ChIP-seq (H3K27me3) analyses of sperm from young (3 months old) vs. aged (21-24 months old) mice (young, *n* = 6 mice; old, *n* = 4 mice). Annotation of all differential histone post-translational modifications (significant results were obtained for H3K27me3 only; FDR < 0.1). Columns 'Chr', 'Start', 'End' and 'Strand' contain the genomic location of each dhPTM using mm10 genome assembly as reference. The column 'Annotation' shows the genomic structure where the dhPTM is located and other columns are annotations of the closest gene (TSS).

Chromosome	Start	End	Gene Symbol	UCSC ID	Distance (bp)	Methylation difference	P value	FDR
					to TSS	old-young		
chr1	168611976	168613976	Fmo9	uc007dkq.1	0	0.166667	0	0
chr11	82805332	82807332	Slfn9	uc007kob.1	0	0.035714	0	0
chr13	55884939	55886939	AK019623	uc007qsa.1	0	0.1	0	0
chr13	55884939	55886939	Catsper3	uc007qsb.1	0	0.1	0	0
chr13	120275845	120277845	Gm7120	uc007rzl.1	0	0.084288	0	0
chr13	120275845	120277845	EG633640	uc007rzm.1	0	0.084288	0	0
chr7	14035189	14037189	Bsph1	uc009ffw.1	0	-0.0625	0	0
chrX	7149725	7151725	Ppp1r3f	uc009slj.1	0	-0.09805	0	0
chrX	7149725	7151725	4930524L23Rik	uc009slk.2	0	-0.09805	0	0
chrX	8776098	8778098	Lancl3	uc009spo.1	0	-0.086703	0	0
chrX	19635695	19637695	Chst7	uc009sss.1	0	-0.109364	0	0
chrX	39501588	39503588	Stag2	uc009taw.1	0	-0.106489	0	0
chrX	39501588	39503588	SAP2	uc009tay.1	0	-0.106489	0	0
chrX	39502877	39504877	Stag2	uc009taw.1	288	-0.104031	0	0
chrX	39502877	39504877	SAP2	uc009tay.1	17	-0.104031	0	0
chrX	57657156	57659156	Atp11c	uc009tib.1	0	-0.084759	0	0
chrX	66612505	66614505	Aff2	uc009tjb.1	0	-0.116039	0	0
chrX	70883779	70885779	Dusp9	uc009tmb.1	0	-0.1556	0	0
chrX	97015407	97017407	Tmem28	uc009tvn.1	0	-0.097612	0	0
chrX	147480775	147482775	Fgd1	uc009uow.1	0	-0.121859	0	0
chrX	154481042	154483042	Cnksr2	uc009ush.1	0	-0.071266	0	0.000001
chrX	53983963	53985963	Fhl1	uc009tgm.1	0	-0.101397	0	0.000015
chrX	53984133	53986133	Fhl1	uc009tgm.1	0	-0.101397	0	0.000015
chr13	120276666	120278666	3110070M22Rik	uc007rzk.2	0	0.071017	0	0.000051
chr13	120276666	120278666	Gm7120	uc007rzl.1	0	0.071017	0	0.000051
chr13	120276666	120278666	EG633640	uc007rzm.1	0	0.071017	0	0.000051
chr12	3234790	3236790	1700012B15Rik	uc007mwj.2	0	0.05584	0	0.000077
chrX	68616934	68618934	Mtmr1	uc009tjt.1	0	-0.106958	0	0.000094
chrX	99043723	99045723	Nhsl2	uc009tyh.1	0	-0.059296	0	0.000096
chrX	136596417	136598417	Nup62cl	uc009ukv.2	0	-0.097124	0	0.0001
chrX	136596417	136598417	E230019M04Rik	uc009ukw.1	0	-0.097124	0	0.0001
chrX	160513981	160515981	Siah1b	uc009uvd.1	0	-0.084141	0	0.000121
chr2	32237435	32239435	1110008P14Rik	uc008jfk.2	0	0.076585	0	0.000158
chr6	83744151	83746151	AK084646	uc012eob.1	0	-0.024146	0	0.000241
chr6	83744151	83746151	Nagk	uc009coh.2	0	-0.024146	0	0.000241
chr13	74454774	74456774	Pdcd6	uc007rey.2	0	0.063527	0	0.000247
chr5	72950884	72952884	Nfxl1	uc008xrl.1	0	0.059998	0	0.000252
chr8	13287012	13289012	Dcun1d2	uc009kxg.1	0	-0.026856	0	0.000252
chr8	13287012	13289012	Tmco3	uc009kxm.1	0	-0.026856	0	0.000252
chr6	83744050	83746050	AK084646	uc012eob.1	0	-0.02423	0.000001	0.000256
chr6	83744050	83746050	Nagk	uc009coh.2	0	-0.02423	0.000001	0.000256
chrX	5976262	5978262	Shroom4	uc009sky.1	0	-0.061053	0.000001	0.000281
chrX	74755565	74757565	Tbl1xr1	uc008osw.1	0	-0.061412	0.000001	0.000282
chrX	33867403	33869403	Lonrf3	uc009sxn.1	0	-0.066246	0.000001	0.000366
chrX	68915941	68917941	Gpr50	uc009tke.1	0	-0.075654	0.000001	0.000371
chr1	94370335	94372335	Ndufa10	uc007cbh.1	0	-0.02312	0.000001	0.000391
chr9	82869096	82871096	Phip	uc009qvv.1	0	-0.024996	0.000002	0.00064
chr11	102046570	102048570	Lsm12	uc007lqs.1	0	-0.060739	0.000002	0.000724
chr1	39043658	39045658	Pdcl3	uc007atc.1	0	-0.02399	0.000002	0.000733
chr1	4846774	4848774	Tcea1	uc007afi.2	0	-0.020947	0.000002	0.000751

Table S7: **Reduced representation bisulfite sequencing (RRBS) identified differentially methylated promoters in old father offspring tissue.** RRBS analyses, using hippocampal tissue of 4-weeks-old young and old father offspring mice as starting material (pooling equimolar amounts of DNA of *n* = 10 mice from 10 litters per group), revealed a set of differentially methylated promoters in old father offspring mice. The table shows the top of the list of genes with differentially methylated promoter regions. Shown are genomic coordinates, gene IDs, methylation differences (old – young), *P* values and false discovery rates (FDR).

Upstream Regulators	P value of overlap	Molecule Type	Predicted Activation
CTCF	7.74E-07	transcription regulator	
RICTOR	7.20E-06	other	
ID2	7.95E-06	transcription regulator	
RAD21	8.55E-06	transcription regulator	
5-azacytidine	2.70E-05	chemical drug	
rapamycin	1.14E-04	chemical drug	Inhibited
ID3	1.19E-04	transcription regulator	
kainic acid	1.37E-04	chemical toxicant	Activated
CDKN3	1.66E-04	phosphatase	
HNF4A	1.68E-04	transcription regulator	
HSF1	2.90E-04	transcription regulator	
1,2-dithiol-3-thione	3.01E-04	chemical reagent	Activated
black raspberry extract	3.10E-04	chemical drug	
ZFP57	3.13E-04	transcription regulator	
plicamycin	3.37E-04	chemical drug	
POU3F2	3.37E-04	transcription regulator	
HTT	4.07E-04	transcription regulator	
TP53	4.15E-04	transcription regulator	Activated
BDNF	4.79E-04	growth factor	Activated
EIF4E	5.61E-04	translation regulator	Activated
Vegf	6.79E-04	group	
flavokawain B	7.07E-04	chemical - endogenous non-mammalian	
CREB1	8.05E-04	transcription regulator	Activated
dexamethasone	8.43E-04	chemical drug	
HIF3A	8.75E-04	transcription regulator	

Top Causal Networks	P value	Predicted activation
PHLPP2	1.16E-13	
PTPRO	1.30E-13	Inhibited
CBLC	4.09E-13	Inhibited
aurinitricarboxylic acid	2.82E-12	Activated
Creb	4.08E-12	Activated

Top Diseases and Disorders	P value
Cancer	1.14E-02 - 8.62E-19
Organismal Injury and Abnormalities	1.15E-02 - 8.62E-19
Gastrointestinal Disease	9.65E-03 - 3.60E-17
Developmental Disorder	1.14E-02 - 2.64E-11
Hereditary Disorder	1.01E-02 - 2.64E-11

Top Molecular and Cellular Functions	P value
Cellular Growth and Proliferation	1.19E-02 - 1.34E-12
Cell Death and Survival	1.09E-02 - 9.81E-11
Cell-To-Cell Signaling and Interaction	8.79E-03 - 5.17E-10
Cellular Assembly and Organization	1.10E-02 - 5.17E-10
Cellular Development	1.19E-02 - 2.20E-08

Top Physiological System Development and Function	P value
Organismal Survival	4.46E-03 - 2.72E-10
Nervous System Development and Function	1.19E-02 - 5.17E-10
Tissue Morphology	1.15E-02 - 5.17E-10
Tissue Development	1.19E-02 - 2.65E-05
Organismal Development	1.08E-02 - 2.89E-05

Table S8: **Pathways, regulators and processes enriched in the gene set with differentially methylated promoters in old father offspring tissue.** The tables show the results of a pathway analysis focusing on the gene set with differentially methylated promoters in old father offspring tissue ($P < 0.05$). They identify upstream regulators predicted to regulate genes with differentially methylated promoters (*P* values indicate significance of overlap; shown is also the predicted activation state of the regulator with its gene set), top causal networks predicted to regulate genes with differentially methylated promoters, top diseases and disorders, top molecular and cellular functions, as well as top physiological system development processes and functions with significant enrichment among differentially methylated promoters in aged sperm (*P* values refer to *P* value ranges, minimal to maximal, of sub-items within the respective category).

Entrez ID	Gene Symbol	LogFC (OFO/YFO)	P Value	FDR
17528	Mpz	5.51	1.90E-19	3.23E-15
20296	Ccl2	2.74	2.43E-09	2.06E-05
13107	Cyp2f2	1.95	4.15E-08	2.35E-04
434794	Xlr4a	-3.10	6.75E-08	2.86E-04
15006	H2-Q1	1.33	6.18E-07	2.10E-03
64378	Gpr88	0.94	6.32E-06	1.79E-02
67639	4930474N09Rik	-3.87	1.07E-05	2.60E-02
20518	Slc22a2	1.05	2.06E-05	3.72E-02
19661	Rbp3	1.46	2.11E-05	3.72E-02
56221	Ccl24	1.72	2.19E-05	3.72E-02
15160	Serpind1	0.78	2.45E-05	3.78E-02
12873	Cpa3	1.42	3.25E-05	4.60E-02
16165	Il13ra2	1.14	4.10E-05	5.36E-02
100040591	Kcnj13	0.96	5.41E-05	6.07E-02
13507	Dsc3	0.81	5.56E-05	6.07E-02
14695	Gnb3	1.64	5.72E-05	6.07E-02
66715	Henmt1	0.69	8.94E-05	8.93E-02
14960	H2-Aa	0.93	1.01E-04	9.55E-02
216350	Tspan8	1.41	1.37E-04	1.22E-01
211577	Mrgprf	0.69	1.80E-04	1.52E-01
629147	Ctxn3	0.74	1.98E-04	1.60E-01
27047	Omd	0.74	2.11E-04	1.62E-01
12160	Bmp5	0.87	2.63E-04	1.92E-01
20306	Ccl7	1.56	2.72E-04	1.92E-01
11889	Asgr1	0.87	2.97E-04	1.96E-01
22626	Slc23a3	1.26	3.00E-04	1.96E-01
71934	Car13	0.81	3.19E-04	2.00E-01
71690	Esm1	1.37	3.77E-04	2.25E-01
108995	Tbc1d10c	-0.86	3.86E-04	2.25E-01
22351	Vill	0.73	3.98E-04	2.25E-01
17196	Mbp	-0.39	4.43E-04	2.43E-01
329366	4932418E24Rik	-0.88	4.69E-04	2.49E-01
208890	Slc26a7	1.21	5.37E-04	2.76E-01
234684	Lrrc29	-0.62	6.25E-04	2.99E-01
12904	Crabp2	0.70	6.37E-04	2.99E-01
15957	Ifit1	0.64	6.43E-04	2.99E-01
16952	Anxa1	0.64	6.52E-04	2.99E-01
381741	Lrrc43	-0.73	7.35E-04	3.28E-01
14264	Fmod	0.92	7.56E-04	3.29E-01
18295	Ogn	0.83	7.85E-04	3.33E-01
14181	Fgfbp1	1.09	1.04E-03	4.23E-01
21804	Tgfb1i1	-0.39	1.05E-03	4.23E-01
208164	Fam180a	0.75	1.07E-03	4.24E-01
17116	Mab21l1	0.79	1.11E-03	4.27E-01
13113	Cyp3a13	-0.70	1.15E-03	4.32E-01
320460	Vwc2l	0.51	1.21E-03	4.45E-01
13836	Epha2	-0.66	1.35E-03	4.87E-01
69983	Sis	-1.11	1.46E-03	5.01E-01
381560	Xkr8	0.39	1.47E-03	5.01E-01
170484	Nphs2	0.90	1.54E-03	5.01E-01

Table S9: **RNA-seq-based assessment of differential gene expression in young and old father offspring tissue.** The table shows the top differentially expressed genes identified in the context of RNA-seq-based differential expression analyses of young and old father offspring mice (hippocampus of 4 weeks old mice as starting material; YFO, *n* = 6 mice from 6 litters; OFO, *n* = 6 mice from 6 litters). Shown are gene IDs, $\log_2$ fold changes (old father offspring / young father offspring), *P* values and false discovery rates (FDR).

Entrez ID	Gene Symbol	LogFC (old/young)	P value	FDR
11522	Adh1	1.74	5.37E-22	9.85E-18
14960	H2-Aa	2.15	7.91E-19	7.26E-15
12010	B2m	1.25	6.86E-17	4.20E-13
100034251	Gm11428	2.68	2.16E-15	9.93E-12
13040	Ctss	2.03	1.52E-14	5.59E-11
18295	Ogn	1.31	3.50E-11	1.07E-07
53328	Pgrmc1	0.78	1.20E-10	3.15E-07
13646	Klk1b22	-2.41	2.55E-10	5.86E-07
17105	Lyz2	2.23	5.58E-10	1.14E-06
17476	Mpeg1	0.96	1.06E-09	1.95E-06
278180	Vsig4	3.54	1.93E-09	3.23E-06
17110	Lyz1	2.34	3.77E-09	5.78E-06
404289	Vmn1r181	1.88	5.27E-09	7.45E-06
14969	H2-Eb1	1.97	1.07E-08	1.40E-05
23972	Papss2	1.39	1.96E-08	2.40E-05
56726	Sh3bgrl	1.07	2.51E-08	2.88E-05
19241	Tmsb4x	0.67	3.18E-08	3.44E-05
58226	Cacna1h	-0.60	4.14E-08	4.23E-05
13058	Cybb	1.65	6.18E-08	5.67E-05
14758	Gpm6b	0.78	6.14E-08	5.67E-05
14961	H2-Ab1	0.95	6.69E-08	5.85E-05
14964	H2-D1	1.21	1.70E-07	0.00014211
20834	Znrf4	-0.61	2.48E-07	0.00019769
20307	Ccl8	3.73	3.84E-07	0.00029401
56758	Mbnl1	0.82	4.40E-07	0.00032327
12009	Azi1	-0.65	4.81E-07	0.00033956
16619	Klk1b27	-1.84	9.87E-07	0.00066929
81799	C1qtnf3	0.89	1.02E-06	0.00066929
12450	Ccng1	0.93	1.17E-06	0.00069524
19652	Rbm3	0.68	1.12E-06	0.00069524
68233	1700125D06Rik	-0.60	1.17E-06	0.00069524
216350	Tspan8	1.48	1.70E-06	0.00089607
60440	Iigp1	2.40	1.67E-06	0.00089607
64291	Osbpl1a	-0.58	1.71E-06	0.00089607
66141	Ifitm3	1.25	1.66E-06	0.00089607
11886	Asah1	0.70	1.79E-06	0.00091263
17311	Kitl	0.76	2.10E-06	0.00101378
20229	Sat1	1.12	2.09E-06	0.00101378
110454	Ly6a	1.32	2.82E-06	0.00132883
68339	Ccdc88c	-0.54	3.03E-06	0.00138968
320590	Svopl	2.00	3.46E-06	0.00154897
11815	Apod	1.95	4.27E-06	0.0018596
19058	Ppp3r1	0.67	4.46E-06	0.0018596
243897	Ggn	-0.53	4.39E-06	0.0018596
622402	Akr1c12	1.67	4.80E-06	0.00195899
14609	Gja1	0.59	5.96E-06	0.00234161
239853	Gpr128	1.45	5.99E-06	0.00234161
16149	Cd74	1.90	6.84E-06	0.00261572
11798	Xiap	0.89	7.55E-06	0.00282979
15430	Hoxd10	1.59	8.97E-06	0.00329415

Table S10: **RNA-seq-based assessment of differential gene expression in young vs. old testis.** The table shows the top differentially expressed genes identified in the context of RNA-seq-based differential expression analyses of young (~4 months old, *n* = 2 mice) vs. old (~24 months old; *n* = 2 mice) testis. Shown are Entrez ID, gene symbol, $\log_2$ fold changes (old / young), *P* value and false discovery rate (FDR).

Ensembl ID	Entrez ID	Gene Symbol	LogFC (Tsc2+/-/WT)	P value	FDR
ENSMUSG00000096403	NA	NA	4.34	1.50E-92	3.65E-88
ENSMUSG00000078249	111241	Hmga1-rs1	2.44	3.13E-19	3.83E-15
ENSMUSG00000044533	16898	Rps2	-0.59	4.61E-15	3.75E-11
ENSMUSG00000002496	22084	Tsc2	-0.87	2.11E-13	1.29E-09
ENSMUSG00000036775	26378	Decr2	-0.47	1.18E-11	5.76E-08
ENSMUSG00000075391	NA	NA	1.47	9.40E-08	0.00038252
ENSMUSG00000096847	210573	Tmem151b	0.27	1.42E-07	0.00049565
ENSMUSG00000023046	16012	Igfbp6	0.68	3.12E-07	0.00095147
ENSMUSG00000034681	19826	Rnps1	-0.34	8.28E-07	0.00224584
ENSMUSG00000034614	216505	Pik3ip1	0.39	1.59E-06	0.0038929
ENSMUSG00000017802	67998	Fam134c	0.23	1.07E-05	0.02238314
ENSMUSG00000000126	216795	Wnt9a	-0.80	1.10E-05	0.02238314
ENSMUSG00000047415	238377	Gpr68	0.46	1.61E-05	0.03027192
ENSMUSG00000033382	75964	Trappc8	-0.24	1.93E-05	0.0337444
ENSMUSG00000025277	66082	Abhd6	0.18	2.55E-05	0.04154688
ENSMUSG00000036054	234373	Sugp2	-0.25	2.98E-05	0.04552182
ENSMUSG00000019916	18451	P4ha1	0.55	3.46E-05	0.0497455
ENSMUSG00000028414	246179	Fktn	0.34	4.00E-05	0.05424781
ENSMUSG00000041771	238384	Slc24a4	0.34	4.39E-05	0.05646671
ENSMUSG00000097428	NA	NA	-0.67	5.83E-05	0.0685699
ENSMUSG00000090663	NA	NA	-0.27	5.90E-05	0.0685699
ENSMUSG00000060733	69718	Ipmk	0.33	6.53E-05	0.07138768
ENSMUSG00000026657	209630	Frmd4a	0.32	6.72E-05	0.07138768
ENSMUSG00000039057	244281	Myo16	-0.49	7.30E-05	0.07423206
ENSMUSG00000020486	18952	Sept4	-0.43	7.87E-05	0.07489319
ENSMUSG00000008136	14200	Fhl2	-0.27	8.69E-05	0.07489319
ENSMUSG00000046711	15361	Hmga1	-0.50	8.69E-05	0.07489319
ENSMUSG00000024130	27410	Abca3	0.29	8.86E-05	0.07489319
ENSMUSG00000021638	18260	Ocln	0.47	8.92E-05	0.07489319
ENSMUSG00000027954	13636	Efna1	0.60	9.30E-05	0.07489319
ENSMUSG00000026864	14828	Hspa5	0.43	9.98E-05	0.07489319
ENSMUSG00000026469	19775	Xpr1	0.27	0.0001004	0.07489319
ENSMUSG00000035372	72056	1810055G02Rik	0.34	0.00010457	0.07489319
ENSMUSG00000022434	73225	Fam118a	0.31	0.00010596	0.07489319
ENSMUSG00000024493	107045	Lars	-0.30	0.00010736	0.07489319
ENSMUSG00000021957	21881	Tkt	-0.17	0.00012212	0.08282195
ENSMUSG00000003200	20405	Sh3gl1	0.25	0.0001288	0.08499091
ENSMUSG00000024991	13669	Eif3a	-0.33	0.00014965	0.09615274
ENSMUSG00000020522	216760	Mfap3	0.46	0.00016046	0.09706953
ENSMUSG00000007038	18010	Neu1	0.17	0.00016136	0.09706953
ENSMUSG00000035401	233545	2210018M11Rik	-0.32	0.00016322	0.09706953
ENSMUSG00000031543	11733	Ank1	-0.37	0.00016698	0.09706953
ENSMUSG00000033623	69587	Pcgf3	0.28	0.00017597	0.09991768
ENSMUSG00000021203	68149	Otub2	0.30	0.00019661	0.1090992
ENSMUSG00000022462	67760	Slc38a2	0.23	0.00021407	0.11614755
ENSMUSG00000036422	18530	Pcdh8	0.34	0.00022236	0.11718945
ENSMUSG00000022314	19357	Rad21	-0.19	0.0002287	0.11718945
ENSMUSG00000003153	20527	Slc2a3	0.19	0.00023039	0.11718945
ENSMUSG00000029804	73998	Herc3	-0.30	0.00023641	0.11779752
ENSMUSG00000082900	NA	NA	-0.98	0.00025146	0.12279179

Table S11: **The Ribotag technology was used to identify genes expressionally regulated, in hippocampal neurons, by a *Tsc2*$^{+/-}$ mutation.** In order to identify genes whose expression is regulated in response to overactive mTOR signaling, we combined the Ribotag approach in αCaMKII-Cre/Ribotag mice, on either a *Tsc2*$^{+/-}$ (associated with overactive mTOR signaling) or WT control background and treated with either the pharmacological mTOR inhibitor rapamycin or vehicle control, with an RNA-seq-based differential expression analysis (rapamycin-treated *Tsc2*$^{+/-}$/αCaMKII-Cre/Ribotag, *n* = 4 mice; vehicle-treated *Tsc2*$^{+/-}$/αCaMKII-Cre/Ribotag, *n* = 3 mice; rapamycin-treated WT/αCaMKII-Cre/Ribotag, *n* = 5 mice; vehicle-treated WT/αCaMKII-Cre/Ribotag, *n* = 5 mice). The table shows the top differentially expressed genes with gene IDs, $\log_2$ fold changes (*Tsc2*$^{+/-}$ / WT), *P* values and false discovery rates (FDR).

Ensembl ID	Entrez ID	Gene Symbol	LogFC (rapamycin/vehicle)	P value	FDR
ENSMUSG00000027035	241447	Cers6	-0.42	2.28E-10	5.57E-06
ENSMUSG00000020362	104625	Cnot6	-0.54	6.13E-10	7.49E-06
ENSMUSG00000045589	230235	Frrs1l	-0.33	1.24E-09	1.01E-05
ENSMUSG00000035614	328108	Fam179b	-0.53	1.77E-09	1.08E-05
ENSMUSG00000025144	20892	Stra13	0.70	9.19E-09	4.49E-05
ENSMUSG00000014498	237615	Ankrd52	-0.54	1.35E-08	5.49E-05
ENSMUSG00000037896	217864	Rcor1	-0.51	1.68E-08	5.87E-05
ENSMUSG00000023232	230779	Serinc2	-0.81	3.95E-08	9.52E-05
ENSMUSG00000040855	194590	Reps2	-0.34	4.09E-08	9.52E-05
ENSMUSG00000037111	73251	Setd7	-0.47	4.25E-08	9.52E-05
ENSMUSG00000023951	22339	Vegfa	0.77	4.29E-08	9.52E-05
ENSMUSG00000025277	66082	Abhd6	-0.27	6.33E-08	0.00011929
ENSMUSG00000037172	243780	E330009J07Rik	-0.40	6.35E-08	0.00011929
ENSMUSG00000092060	666938	Bend4	-0.72	7.31E-08	0.00012755
ENSMUSG00000049470	93736	Aff4	-0.37	9.57E-08	0.00015582
ENSMUSG00000034845	84094	Plvap	0.61	1.02E-07	0.00015605
ENSMUSG00000037104	56468	Socs5	-0.24	1.20E-07	0.00016402
ENSMUSG00000063415	232174	Cyp26b1	-0.91	1.23E-07	0.00016402
ENSMUSG00000008136	14200	Fhl2	0.41	1.29E-07	0.00016402
ENSMUSG00000026623	226856	Lpgat1	-0.31	1.34E-07	0.00016402
ENSMUSG00000031167	19652	Rbm3	0.84	1.98E-07	0.0002299
ENSMUSG00000073755	230757	5730409E04Rik	0.23	2.72E-07	0.00030135
ENSMUSG00000021068	18080	Nin	-0.56	3.24E-07	0.0003443
ENSMUSG00000026322	15562	Htr4	-0.60	4.68E-07	0.00047596
ENSMUSG00000030275	75320	Etnk1	-0.30	5.56E-07	0.0005431
ENSMUSG00000052572	23859	Dlg2	-0.43	6.36E-07	0.00058314
ENSMUSG00000040771	106821	Oard1	0.51	6.45E-07	0.00058314
ENSMUSG00000031652	80750	N4bp1	-0.35	7.61E-07	0.00066383
ENSMUSG00000041132	100637	N4bp2l1	0.49	8.03E-07	0.0006764
ENSMUSG00000005610	13690	Eif4g2	-0.26	8.73E-07	0.00071058
ENSMUSG00000020990	71091	Cdkl1	0.53	1.14E-06	0.0008978
ENSMUSG00000016477	13557	E2f3	-0.38	1.29E-06	0.00098724
ENSMUSG00000046062	108954	Ppp1r15b	-0.29	1.74E-06	0.00128729
ENSMUSG00000021796	12166	Bmpr1a	-0.36	1.86E-06	0.001338
ENSMUSG00000035401	233545	2210018M11Rik	0.46	2.15E-06	0.00146085
ENSMUSG00000036095	217480	Dgkb	-0.38	2.15E-06	0.00146085
ENSMUSG00000022160	56335	Mettl3	-0.57	2.47E-06	0.00160137
ENSMUSG00000018042	109754	Cyb5r3	0.33	2.49E-06	0.00160137
ENSMUSG00000037253	240396	Mex3c	-0.49	2.59E-06	0.00161927
ENSMUSG00000042599	338523	Jhdm1d	-0.60	3.14E-06	0.00189939
ENSMUSG00000064340	NA	NA	1.80	3.19E-06	0.00189939
ENSMUSG00000040084	12236	Bub1b	1.41	3.83E-06	0.00222454
ENSMUSG00000008318	320100	Relt	0.68	3.97E-06	0.00223709
ENSMUSG00000021537	12626	Cetn3	0.40	4.03E-06	0.00223709
ENSMUSG00000020102	20503	Slc16a7	-0.60	4.43E-06	0.0024026
ENSMUSG00000038121	108654	Fam210a	-0.33	4.78E-06	0.00253721
ENSMUSG00000029436	23948	Mmp17	-0.30	5.22E-06	0.00261281
ENSMUSG00000039648	70266	Ccbl1	0.52	5.22E-06	0.00261281
ENSMUSG00000032290	56294	Ptpn9	-0.38	5.24E-06	0.00261281
ENSMUSG00000018669	80280	Cdk5rap3	0.50	5.87E-06	0.00286599

Table S12: **The Ribotag technology was used to identify genes expressionally regulated by rapamycin in hippocampal neurons.** In order to identify genes expressionally regulated in response to inhibited mTOR signaling, we combined the Ribotag approach in αCaMKII-Cre/Ribotag mice, on either a *Tsc2*$^{+/-}$ or WT background and treated with either the pharmacological mTOR inhibitor rapamycin or vehicle control, with an RNA-seq-based differential expression analysis (rapamycin-treated *Tsc2*$^{+/-}$/αCaMKII-Cre/Ribotag, *n* = 4 mice; vehicle-treated *Tsc2*$^{+/-}$/αCaMKII-Cre/Ribotag, *n* = 3 mice; rapamycin-treated WT/αCaMKII-Cre/Ribotag, *n* = 5 mice; vehicle-treated WT/αCaMKII-Cre/Ribotag, *n* = 5 mice). The table shows the top differentially expressed genes with gene IDs, $\log_2$ fold changes (rapamycin / vehicle control), *P* values and false discovery rates (FDR).

Entrez ID	Gene Symbol	LogFC (old/young)	FDR
17105	Lyz2	3.19	0
19144	Klk6	4.27	0
23962	Oasl2	2.09	0
93695	Gpnmb	1.77	0
22041	Trf	1.25	0
14580	Gfap	1.43	0
15957	Ifit1	2.19	0
17110	Lyz1	3.10	0
17476	Mpeg1	1.63	0
20750	Spp1	2.05	0
12260	C1qb	1.38	0
56644	Clec7a	4.49	0
13011	Cst7	4.75	0
13040	Ctss	1.37	0
11815	Apod	1.63	0
22177	Tyrobp	1.46	0
12266	C3	2.86	0
13058	Cybb	3.01	0
16411	Itgax	4.09	0
12268	C4b	2.45	0
23833	Cd52	2.56	0
15959	Ifit3	1.57	0
20716	Serpina3n	1.77	0
104816	Aspg	1.95	0
68794	Flnc	1.77	0
22352	Vim	1.27	0
14728	Lilrb4	3.59	0
12259	C1qa	1.27	0
20200	S100a6	1.41	0
76933	Ifi27l2a	2.49	0
83433	Trem2	1.34	0
12262	C1qc	1.26	0
12514	Cd68	1.50	0
54123	Irf7	1.92	0
18173	Slc11a1	1.94	0
14964	H2-D1	1.20	0
19039	Lgals3bp	1.22	0
21816	Tgm1	3.08	0
17085	Ly9	2.98	0
20302	Ccl3	3.04	0
100038882	Isg15	1.88	0
14275	Folr1	-1.45	0
12267	C3ar1	1.88	0
66141	Ifitm3	1.23	0
16414	Itgb2	1.42	0
12010	B2m	1.08	0
16854	Lgals3	1.63	0
19264	Ptprc	1.49	0.000000001
22139	Ttr	-1.03	0.000000001
12523	Cd84	1.64	0.000000001

Table S13: **Differentially expressed genes in the aged hippocampus.** The table shows the top differentially expressed genes in aged hippocampus (~24 months old; *n* = 2 mice) vs. young hippocampus (~4 months old; *n* = 2 mice) as revealed by an RNA-seq analysis of young vs. old rapamycin or vehicle control-treated animals. Listed are gene IDs, $\log_2$ fold changes (old / young) and false discovery rates (FDR).

Entrez ID	Gene Symbol	LogFC (rapamycin/vehicle)	FDR
73870	4930417O13Rik	1.49	0.000000000
243676	E330021D16Rik	1.66	0.000000000
108043	Chrnb3	1.65	0.000000000
68750	Rreb1	1.19	0.000000000
226040	E030010A14Rik	2.28	0.000000000
50720	Sacs	1.33	0.000000088
70358	Steap1	-1.45	0.000009483
12031	Bc1	1.52	0.000009525
110257	Hba-a2	0.92	0.000013138
71236	Rtdr1	1.20	0.000037990
338346	Gpr21	1.95	0.000038771
18763	Pkd1	0.82	0.000042376
100503605	Beta-s	0.83	0.000055989
630084	Pol	0.79	0.000081849
20370	Sez6	0.77	0.000146641
20665	Sox10	-0.83	0.000185528
17441	Mog	-0.80	0.000196836
71898	Apol9b	3.27	0.000197033
18606	Enpp2	-0.77	0.000197033
71939	Apol6	1.28	0.000259079
14618	Gjb1	-0.94	0.000268432
17105	Lyz2	-0.84	0.000285046
20190	Ryr1	0.78	0.000417728
320429	Trank1	0.73	0.000428137
19144	Klk6	-0.96	0.000473141
23962	Oasl2	1.01	0.000473141
100038882	Isg15	1.24	0.000473141
18417	Cldn11	-0.73	0.000473141
15129	Hbb-b1	0.84	0.000473141
338521	Fa2h	-0.82	0.000473141
100041581	Zkscan16	0.83	0.000544837
12153	mKIAA4159	0.74	0.000544837
17153	Mal	-0.71	0.000592810
93695	Gpnmb	-0.89	0.000603285
18823	Plp1	-0.70	0.000618630
22041	Trf	-0.70	0.000854865
574402	Gpr17	-0.78	0.000897639
68144	5031426D15Rik	0.98	0.000897639
77125	Il33	-0.71	0.001082249
320587	Tmem88b	-0.71	0.001132234
230379	Acer2	0.97	0.001132234
22239	Ugt8a	-0.74	0.001365907
53608	Map3k6	0.93	0.001622770
19090	Prkdc	0.70	0.002264001
63830	Kcnq1ot1	0.68	0.002301681
72690	Grrp1	1.25	0.002301681
12799	Cnp	-0.66	0.002365299
12289	cacna1d	0.69	0.002365299
17136	Mag	-0.66	0.002368330
16177	Il1r1	0.77	0.002495247

Table S14: **Differentially expressed genes in response to rapamycin treatment.** The table shows the top differentially expressed genes in the hippocampus of rapamycin-treated animals (*n* = 2 mice) vs. vehicle control mice (*n* = 2 mice) as identified by an RNA-seq analysis of young (~4 months) vs. old (~24 months) rapamycin or vehicle control-treated animals. Shown are gene IDs, $\log_2$ fold changes (old / young) and false discovery rates (FDR).